CONFLICT OF INTEREST

The authors state no conflict of interest.

ACKNOWLEDGMENTS

We thank Mery Clausen (Gene Therapy Institute, Hadassah Hospital) for technical assistance. This study was supported by the Horwitz Foundation, the Israeli Ministry of Science – the Knowledge Center for Gene Therapy, the Blum Foundation, and the Grinspoon Foundation.

REFERENCES

Aiuti A, Webb IJ, Bleul C, Springer T, Gutierrez-Ramos JC (1997) The chemokine SDF-1 is a chemoattractant for human CD34+ hematopoietic progenitor cells and provides a new mechanism to explain the mobilization of CD34+ progenitors to peripheral blood. *J Exp Med* 185:111–20

Askari AT, Unzek S, Popovic ZB, Goldman CK, Forudi F, Kiedrowski M *et al.* (2003) Effect of stromal-cell-derived factor 1 on stem-cell homing and tissue regeneration in ischaemic cardiomyopathy. *Lancet* 362:697–703

Ceradini DJ, Kulkarni AR, Callaghan MJ, Tepper OM, Bastidas N, Kleinman ME *et al.* (2004) Progenitor cell trafficking is regulated by hypoxic gradients through HIF-1 induction of SDF-1. *Nat Med* 10:858–64

Clark RA (1988) *The molecular and cellular biology of wound repair*, 2nd ed. New York: Kluwer Academic Plenum Publishers

Cotran RS, Kumar V, Collins T (1999) *Pathologic basis of disease*, 6th ed. Philadelphia: W.B. Saunders Company

Doitsidou M, Reichman-Fried M, Stebler J, Koprunner M, Dorries J, Meyer D *et al.* (2002) Guidance of primordial germ cell migration by the chemokine SDF-1. *Cell* 111:647–59

Faunce DE, Llanas JN, Patel PJ, Gregory MS, Duffner LA, Kovacs EJ (1999) Neutrophil chemokine production in the skin following scald injury. *Burns* 25:403–10

Gibran NS, Ferguson M, Heimbach DM, Isik FF (1997) Monocyte chemoattractant protein-1 mRNA expression in the human burn wound. *J Surg Res* 70:1–6

Gillitzer R, Goebeler M (2001) Chemokines in cutaneous wound healing. *J Leukocyte Biol* 69:513–21

Gonzalo JA, Lloyd CM, Peled A, Delaney T, Coyle AJ, Gutierrez-Ramos JC (2000) Critical involvement of the chemotactic axis CXCR4/stromal cell-derived factor-1 α in the inflammatory component of allergic airway disease. *J Immunol* 165:499–508

Green H, Kehinde O, Thomas J (1979) Growth of cultured human epidermal cells into multiple epithelia suitable for grafting. *Proc Natl Acad Sci USA* 76:5665–8

Hitchon C, Wong K, Ma G, Reed J, Lyttle D, El-Gabalawy H (2002) Hypoxia-induced production of stromal cell-derived factor 1 (CXCL12) and vascular endothelial growth factor by synovial fibroblasts. *Arthritis Rheum* 46:2587–97

Iocono JA, Colleran KR, Remick DG, Gillespie BW, Ehrlich HP, Garner WL (2000) Interleukin-8 levels and activity in delayed-healing human thermal wounds. *Wound Repair Regen* 8:216–25

Lukacs NW, Berlin A, Schols D, Skerlj RT, Bridger GJ (2002) AMD3100, a CXCR4 antagonist, attenuates allergic lung inflammation and airway hyperreactivity. *Am J Pathol* 160:1353–60

Ma Q, Jones D, Borghesani PR, Segal RA, Nagasawa T, Kishimoto T *et al.* (1998) Impaired B-lymphopoiesis, myelopoiesis, and derailed cerebellar neuron migration in CXCR4- and SDF-1-deficient mice. *Proc Natl Acad Sci USA* 95:9448–53

McGrath KE, Koniski AD, Maltby KM, McGann JK, Palis J (1999) Embryonic expression and function of the chemokine SDF-1 and its receptor, CXCR4. *Dev Biol* 213:442–56

Nagasawa T, Hirota S, Tachibana K, Takakura N, Nishikawa S, Kitamura Y *et al.* (1996) Defects of B-cell lymphopoiesis and bone-marrow myelopoiesis in mice lacking the CXC chemokine PBSF/SDF-1. *Nature* 382:635–8

Nagase H, Kudo K, Izumi S, Ohta K, Kobayashi N, Yamaguchi M *et al.* (2001a) Chemokine receptor expression profile of eosinophils at inflamed tissue sites: decreased CCR3 and increased CXCR4 expression by lung eosinophils. *J Allergy Clin Immunol* 108:563–9

Nagase H, Miyamasu M, Yamaguchi M, Fujisawa T, Kawasaki H, Ohta K *et al.* (2001b) Regulation of chemokine receptor expression in eosinophils. *Int Arch Allergy Immunol* 125:1129–32

Nagase H, Miyamasu M, Yamaguchi M, Fujisawa T, Ohta K, Yamamoto K *et al.* (2000) Expression of CXCR4 in eosinophils: functional analyses and cytokine-mediated regulation. *J Immunol* 164:5935–43

Ono I, Gunji H, Zhang JZ, Maruyama K, Kaneko F (1995) A study of cytokines in burn blister fluid related to wound healing. *Burns* 21: 352–5

Pablos JL, Amara A, Bouloc A, Santiago B, Caruz A, Galindo M *et al.* (1999) Stromal-cell derived factor is expressed by dendritic cells and endothelium in human skin. *Am J Pathol* 155:1577–86

Peled A, Petit I, Kollet O, Magid M, Ponomaryov T, Byk T *et al.* (1999) Dependence of human stem cell engraftment and repopulation of NOD/SCID mice on CXCR4. *Science* 283:845–8

Petit I, Szyper-Kravitz M, Nagler A, Lahav M, Peled A, Hablea L *et al.* (2002) G-CSF induces stem cell mobilization by decreasing bone marrow SDF-1 and up-regulating CXCR4. *Nat Immunol* 3:687–94

Piccolo MT, Wang Y, Verbrugge S, Warner RL, Sannomiya P, Piccolo NS *et al.* (1999) Role of chemotactic factors in neutrophil activation after thermal injury in rats. *Inflammation* 23:371–85

Ponomaryov T, Peled A, Petit I, Taichman RS, Habler L, Sandbank J *et al.* (2000) Induction of the chemokine stromal-derived factor-1 following DNA damage improves human stem cell function. *J Clin Invest* 106:1331–9

Qu C, Edwards EW, Tacke F, Angeli V, Llodra J, Sanchez-Schmitz G *et al.* (2004) Role of CCR8 and other chemokine pathways in the migration of monocyte-derived dendritic cells to lymph nodes. *J Exp Med* 200: 1231–41

Schioppa T, Uranchimeg B, Saccani A, Biswas SK, Doni A, Rapisarda A *et al.* (2003) Regulation of the chemokine receptor CXCR4 by hypoxia. *J Exp Med* 198:1391–402

Singer AJ, Clark RA (1999) Cutaneous wound healing. *N Engl J Med* 341:738–46

Smith JM, Johanesen PA, Wendt MK, Binion DG, Dwinell MB (2005) CXCL12 activation of CXCR4 regulates mucosal host defense through stimulation of epithelial cell migration and promotion of intestinal barrier integrity. *Am J Physiol Gastrointest Liver Physiol* 288:316–26

Spies M, Dasu MR, Svrakic N, Nesic O, Barrow RE, Perez-Polo JR *et al.* (2002) Gene expression analysis in burn wounds of rats. *Am J Physiol Regul Integr Comp Physiol* 283:918–30

Struzyna J, Pojda Z, Braun B, Chomicka M, Sobiczewska E, Wrembel J (1995) Serum cytokine levels (IL-4, IL-6, IL-8, G-CSF, GM-CSF) in burned patients. *Burns* 21:437–40

Tamamura H, Hori A, Kanzaki N, Hiramatsu K, Mizumoto M, Nakashima H *et al.* (2003) T140 analogs as CXCR4 antagonists identified as anti-metastatic agents in the treatment of breast cancer. *FEBS Lett* 550:79–83

Wald O, Pappo O, Safadi R, Dagan-Berger M, Beider K, Wald H *et al.* (2004) Involvement of the CXCL12/CXCR4 pathway in the advanced liver disease that is associated with hepatitis C virus or hepatitis B virus. *Eur J Immunol* 34:1164–74

Yang J, Torio A, Donoff RB, Gallagher GT, Egan R, Weller PF *et al.* (1997) Depletion of eosinophil infiltration by anti-IL-5 monoclonal antibody (TRFK-5) accelerates open skin wound epithelial closure. *Am J Pathol* 51:1813–9

Zou YR, Kottmann AH, Kuroda M, Taniuchi I, Littman DR (1998) Function of the chemokine receptor CXCR4 in haematopoiesis and in cerebellar development. *Nature* 393:595–9

ORGANIC LETTERS
2006
Vol. 8, No. 4
613–616

Unequivocal Synthesis of (*Z*)-Alkene and (*E*)-Fluoroalkene Dipeptide Isosteres To Probe Structural Requirements of the Peptide Transporter PEPT1

Ayumu Niida,[†] Kenji Tomita,[†] Makiko Mizumoto,[†] Hiroaki Tanigaki,[†] Tomohiro Terada,[‡] Shinya Oishi,[†] Akira Otaka,[†,§] Ken-ichi Inui,[‡] and Nobutaka Fujii*,[†]

Graduate School of Pharmaceutical Sciences, Kyoto University, Sakyo-ku, Kyoto 606-8501, Japan, Department of Pharmacy, Kyoto University Hospital, Sakyo-ku, Kyoto 606-8507, Japan, and Graduate School of Pharmaceutical Sciences, The University of Tokushima, Tokushima 770-8505, Japan

nfujii@pharm.kyoto-u.ac.jp

Received November 17, 2005

ABSTRACT

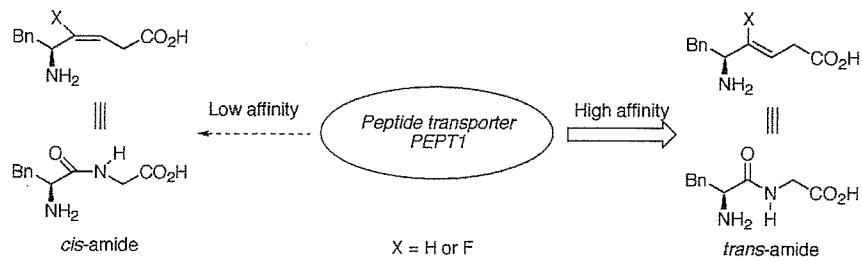

Described is a novel synthetic route for dipeptide isosteres containing (*Z*)-alkene and (*E*)-fluoroalkene units as *cis*-amide bond equivalents via organocopper-mediated reduction of γ-acetoxy- or γ,γ-difluoro-α,β-unsaturated-δ-lactams. The synthesized isosteres were evaluated in terms of their affinities for the peptide transporter PEPT1. *trans*-Amide isosteres tended to possess higher affinities for PEPT1 as compared to the corresponding *cis*-amide bond equivalents.

In postgenomic drug discovery research, the rapid elucidation of structural requirements of the ligands for newly identified drug targets (e.g., GPCRs, enzymes, transporters, etc.) is strongly needed in the arena of medicinal chemistry.[1] Many protein drug targets interact with proteinic or peptidic ligands. Therefore, development of peptidomimetic small molecules is important for investigating criteria for the mutual molecular recognition.[2] Alkene-type dipeptide isosteres represent potential amide bond mimetics (Figure 1).[3] Fluoroalkene dipeptide isosteres were designed as electrostatically favorable mimetics as compared to simple alkene isosteres.[4] These isosteres have structural similarities with the parent peptides

[†] Graduate School of Pharmaceutical Sciences, Kyoto University.
[‡] Kyoto University Hospital.
[§] The University of Tokushima.

(1) (a) Drews, J. *Science* **2000**, *287*, 1960. (b) Klabunde, T.; Hessler, G. *ChemBioChem* **2002**, *3*, 928. (c) Tyndall, J. D. A.; Pfeiffer, B.; Abbenante, G., Fairlie, D. P. *Chem. Rev.* **2005**, *105*, 793.

(2) (a) Burgess, K. *Acc. Chem. Res.* **2001**, 34, 826. (b) Bursavich M. G.; Rich, D. H. *J. Med. Chem.* **2002**, *45*, 541. (c) Hruby, V. J. *J. Med Chem.* **2003**, *46*, 4215.

(3) (a) Oishi, S.; Kamano, T.; Niida, A.; Odagaki, Y.; Hamanaka, N.; Yamamoto, M.; Ajito, K.; Tamamura, H.; Otaka, A.; Fujii, N. *J. Org. Chem.* **2002**, *67*, 6162. (b) Wipf, P.; Xiao, J. *Org. Lett.* **2005**, *7*, 103. (c) Xiao, J.; Weisblum, B.; Wipf, P. *J. Am. Chem. Soc.* **2005**, *127*, 5742.

(4) (a) Abraham, R. J.; Ellison, S. L. R.; Schonholzer, P.; Thomas, W. A. *Tetrahedron* **1986**, *42*, 2101. (b) Allmendinger, T.; Furet, P.; Hungerbühler, E.; *Tetrahedron Lett.* **1990**, *31*, 7297. (c) Allmendinger, T.; Furet, P.; Hungerbühler, E.; *Tetrahedron Lett.* **1990**, *31*, 7301. (d) Otaka, A.; Watanabe, J.; Yukimasa, A.; Sasaki, Y.; Watanabe, H.; Kinoshita, T.; Oishi, S.; Tamamura, H.; Fujii, N. *J. Org. Chem.* **2004**, *69*, 1634. (e) V. d. Veken, P.; Senten, K.; Kertèsz, I.; D. Meester, I.; Lambeir, A.-M.; Maes, M.-B.; Scharpè, S.; Haemers, A.; Augustyns, K. *J. Med. Chem.* **2005**, *48*, 1768. (f) Nakamura, Y.; Okada, M.; Sato, A.; Horikawa, H.; Koura, M.; Saito, A.; Taguchi, T. *Tetrahedron* **2005**, *61*, 5741.

10.1021/ol052781k CCC: $33.50
Published on Web 01/24/2006

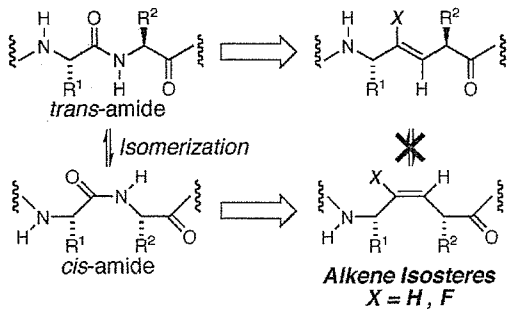

Figure 1. *Cis*/*trans* equilibrium of peptide bond and the corresponding alkene- or fluoroalkene isosteres.

and resist enzymatic degradation. Peptide bonds exist in *cis*/*trans* equilibrium, while alkene isosteres serve as defined *trans*-amide or *cis*-amide equivalents, which do not isomerize to each other. *Cis*/*trans* isomerization of peptide bonds (especially Xaa-Pro sequences) in several bioactive peptides tends to play an important role in their conformations and biological activities.[5] Therefore, alkene and fluoroalkene isosteres might be promising tools for conformational analysis of bioactive peptides and proteins.[6] We have been engaged in the development of synthetic methodologies for (*E*)-alkene or (*Z*)-fluoroalkene dipeptide isosteres as *trans*-amide bond equivalents utilizing organocopper reagents or SmI_2. However, the lack of efficient synthetic methodologies for the preparation of (*Z*)-alkene or (*E*)-fluoroalkene dipeptide isosteres as *cis*-amide bond equivalents has limited an extensive application of alkene and fluoroalkene isosteres in the analysis of amide bond geometries in bioactive peptides and proteins. In this paper, we describe a new synthetic approach for the preparation of (*Z*)-alkene or (*E*)-fluoroalkene dipeptide isosteres. We also include the application of these isosteres to probe structural requirements of the peptide transporter PEPT1.

Our synthetic routes for the preparation of (*Z*)-alkene and (*E*)-fluoroalkene isosteres are depicted in Scheme 1. We envisioned key synthetic intermediates **B** would be synthesized by organocopper-mediated reduction of lactam **A** with predominant formation of β,γ-(*Z*)-alkenes or (*E*)-fluoroalkenes as *cis*-amide equivalents. This strategy could be expanded into consecutive one-pot reduction/α-alkylation methodologies for the synthesis of structurally diverse α-alkylated (*Z*)-alkene and (*E*)-fluoroalkene dipeptide isosteres.[7] First, we synthesized γ-acetoxy- or γ,γ-difluoro-α,β-unsaturated lactams and examined the organocopper-mediated reduction of these substrates to confirm whether this approach was applicable to the synthesis of *cis*-amide bond isosteres.

Guibé et al. reported a similar but inherently different convergent approach to the synthesis of (*Z*)-alkene isosteres

Scheme 1. Synthetic Route for (*Z*)-Alkene and (*E*)-Fluoroalkene Dipeptide Isosteres

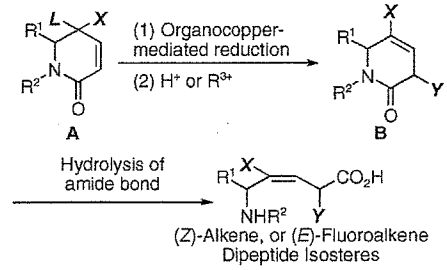

L: leaving group (OAc or F). *X*: H or F. *Y*: H or R^3.

via 3,6-dihydropyridin-2-ones, in which the β,γ-(*Z*)-alkene unit was constructed by Grubbs' RCM after condensation of chiral allylamines with chiral vinyl acetic acids.[8] The present method provides a new entity for the synthesis of (*Z*)-alkene isosteres in a divergent fashion. That is complementary to their method as well as our alternative method based on organocoper-mediated *anti*-S_N2' reaction.[9] It is noteworthy that to our knowledge, this is the first unequivocal synthesis of (*E*)-fluoroalkene dipeptide isosteres.

Substrates for the organocopper-mediated reduction were synthesized by the sequence of reactions shown in Scheme 2. Synthesis of acetate **6** started from a known phenylalanine derivative **1**.[9] Conversion of the *N*-protecting group of **1** to *N*-Ns (Ns = 2-nitrobenzenesulfonyl)[10] followed by *O*-protection with a TBS group gave *N*-Ns amide derivative **2**. Treatment of **2** with DMB (2,4-dimethoxybenzyl) alcohol under Mitsunobu conditions afforded the *N*-DMB sulfonamide **3**. After removal of the *N*-Ns group of **3**, acylation of the resulting secondary amine followed by *O*-TBS deprotection gave the acrylamide derivative **4**. RCM reaction of **4** with Grubbs' ruthenium catalyst[11] proceeded smoothly at room temperature to yield the γ-hydroxy-α,β-unsaturated δ-lactam **5**. Lactam **5** was converted to acetate **6** by Ac_2O treatment in the presence of pyridine.

γ,γ-Difluoro-α,β-unsaturated δ-lactam **12** was synthesized from the β-amino ester **10**, which was prepared from phenylacetaldehyde **7** and the chiral amine **8** via rhodium catalized diastereoselective Reformatsky–Honda reaction.[4d,12] After DIBAL-H treatment of **10**, (*Z*)-selective Horner–Wadsworth–Emmons reaction[13] of the resulting aldehyde gave (*Z*)-enoate **11** in 72% yield with a concomitant formation of small amount of (*E*)-isomer (4%). After deprotection of the Boc and *t*-Bu groups of **11** using 4 M HCl in dioxane, cyclization with EDC gave the desired lactam **12**.

(5) Dugave, C.; Demange, L. *Chem. Rev.* **2003**, *103*, 2475.
(6) Wang, X. J.; Xu, B.; Mullins, A. B.; Neiler, F. K.; Etzkorn, F. A. *J. Am. Chem. Soc.* **2004**, *126*, 15533.
(7) Otaka, A.; Watanabe, H.; Yukimasa, A.; Oishi, S.; Tamamura, H.; Fujii, N. *Tetrahedron Lett.* **2001**, *42*, 5443, and references cited thererin.
(8) Boucard, V.; S.-Dorizon, H.; Guibé, F. *Tetrahedron* **2002**, *58*, 7275.
(9) Niida, A.; Oishi, S.; Sasaki, Y.; Mizumoto, M.; Tamamura, H.; Fujii, N.; Otaka, A. *Tetrahedron Lett.* **2005**, *46*, 4183.
(10) Fukuyama, T.; Jow, C.-K.; Cheung, M. *Tetrahedron Lett.* **1995**, *36*, 6373.
(11) Scholl, M.; Ding, S.; Lee, C. W.; Grubbs, R. H. *Org. Lett.* **1999**, *1*, 953.
(12) Honda, T.; Wakabayashi, H.; Kanai, K. *Chem. Pharm. Bull.* **2002**, *50*, 307.
(13) Ando, K.; Oishi, T.; Hirama, M.; Ohno, H.; Ibuka, T. *J. Org. Chem.* **2000**, *65*, 4745.

Scheme 2. Synthesis of Requisite Substrates for Organocopper-Mediated Reduction

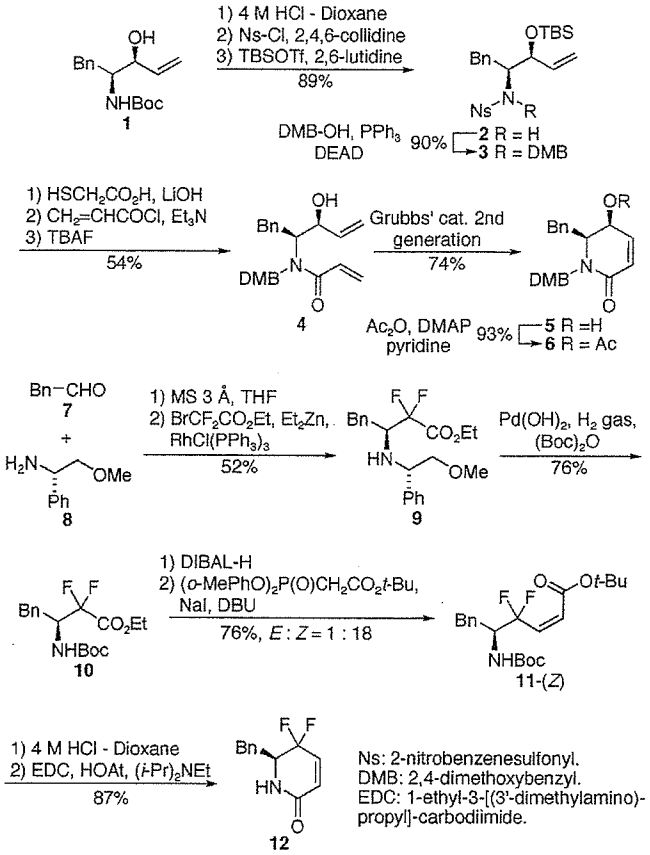

Ns: 2-nitrobenzenesulfonyl.
DMB: 2,4-dimethoxybenzyl.
EDC: 1-ethyl-3-[(3'-dimethylamino)-propyl]-carbodiimide.

Next we examined the organocopper-mediated reduction of lactams **6** and **12** (Scheme 3). The reaction of acetate **6** with Me_3CuLi_2·LiI·3LiBr[14] proceeded smoothly at −78 °C to yield the β,γ-unsaturated lactam **13** in a good yield (88%). The DMB group of lactam **13** was easily removed using TFA. Treatment of difluorolactam **12** with Me_3CuLi_2·LiI·3LiBr also gave the desired reduction product **15** in excellent yield (92%).

Scheme 3. Synthesis of Phe-Gly Type (*Z*)-Alkene- and (*E*)-Fluoroalkene Dipeptide Isosteres via Organocopper-Mediated Reduction of Lactams **6** and **12**

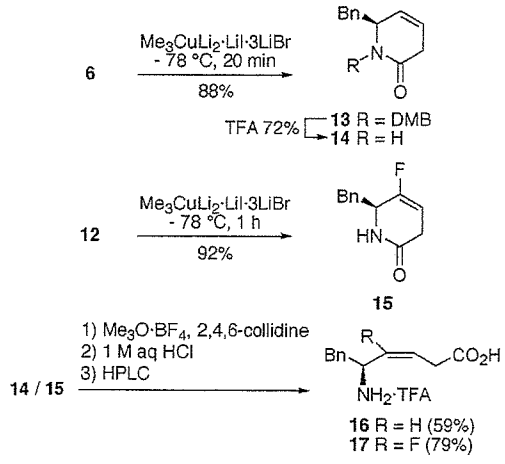

Next, we carried out the hydrolysis of the amide bond in lactams **14** and **15** to accomplish the synthesis of the *cis*-amide bond isosteres. Lactams **14** and **15** were converted to lactim ethers using Me_3O·BF_4. Hydrolysis of the lactim ethers[15] under acidic conditions followed by HPLC purification using 0.1% TFA aqueous MeCN gave Phe-Gly type (*Z*)-alkene dipeptide isostere (Phe-ψ[(*Z*)-CH=CH]-Gly **16**) and (*E*)-fluoroalkene dipeptide isostere (Phe-ψ[(*E*)-CF=CH]-Gly **17**),[16] respectively as TFA salts.

The above organocopper-mediated reduction is applicable to consecutive one-pot α-alkylation (Scheme 4). After

Scheme 4. Synthesis of α-Substituted (*Z*)-Alkene and (*E*)-Fluoroalkene Dipeptide Isosteres Utilizing Organocopper-Mediated Reduction−Alkylation

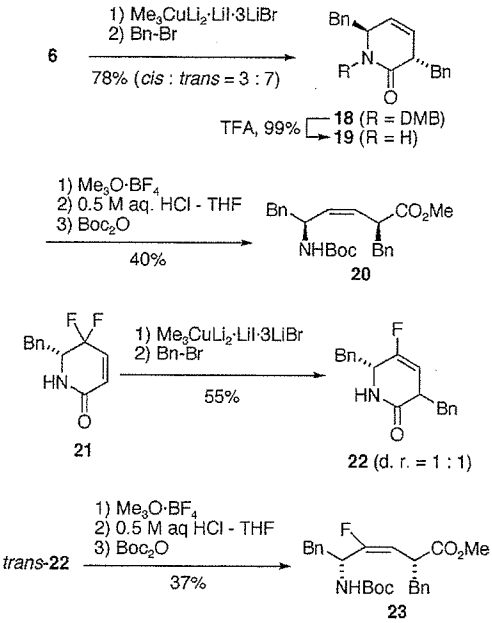

reduction of lactam **6** with Me_3CuLi_2·LiI·3LiBr, the resulting metal enolate was trapped by Bn-Br to yield the *trans*-α-substituted diketopiperazine mimetic **18** as a main product. After deprotection of the DMB group using TFA, the resulting lactam **19** was subjected to ring-opening followed by *N*-Boc protection to yield Boc-L-Phe-ψ[(*Z*)-CH=CH]-D-Phe-OMe **20** in 40% yield with a small amount of α-epimerized product (13%). Boc-D-Phe-ψ[(*E*)-CF=CH]-L-Phe-OMe **23** was also synthesized from lactam **21** by a procedure

(14) Single electron transfer (SET) mechanism has been proposed as one of the plausible mechanisms of organocopper-mediated reduction. The electron-transfer potency of Me_3CuLi_2 was proved to be higher than that of the corresponding Gilman-type reagent such as Me_2CuLi. See: Chounan, Y.; Horino, H.; Ibuka, T.; Yamamoto, Y. *Bull. Chem. Soc. Jpn.* **1997**, *70*, 1953.

(15) Schöllkopf, U.; Hartwig, W.; Pospischil, K.-H.; Kehne, H. *Synthesis* **1981**, 966.

(16) Coupling constants of **17** and **23** ($^3J_{HF}$ = 20.7 and 20.5 Hz, respectively) are consistent with those of α-fluorovinyl groups possessing a (*E*)-configuration ($^3J_{HFtrans}$ = 18−22 Hz). See ref 4b.

similar to that for the synthesis of isostere **20**.[17] Precise stereocontrol and introduction of other functional groups at the α-position are under investigation.

Next, we investigated whether the di/tri-peptide transporter, PEPT1 recognized synthetic Phe-Gly type isosteres as substrates. PEPT1 is a membrane protein which has 12 transmembrane domains and mediates intestinal uptake of not only di-/tripeptides but also several drugs structually related to small peptides such as β-lactam antibiotics.[18] Structure−activity relationship studies of various substrates for PEPT1 have been carried out in order to apply this transporter to develop orally bio-available drugs. However precise recognition mechanisms have not been elucidated. We envisioned that alkene dipeptide isosteres would be useful tools for analysis of recognition mechanisms of PEPT1 because of their structural similarity to parent dipeptides. We also expected that the potency of dipeptide isosteres as amide bond mimetics could be evaluated by use of the PEPT1 dipeptide transport system.

The bioactivities of synthetic Phe-Gly isosteres for PEPT1 were determined by the inhibition of [^{3}H]Gly-Sar uptake in PEPT1-expressing Caco-2 cell in comparison with *trans*-amide type isosteres, **24**, **25**, and other related compounds (see the Supporting Information attached). Inhibition constants (K_i) of parent dipeptide Phe-Gly and its isosteres are shown in Table 1. *trans*-Amide equivalents **24** and **25** possessed good affinity for PEPT1 corresponding to the parent dipeptide (K_i: Phe-Gly, 0.205 mM; **24**, 0.853 mM; **25**, 1.34 mM). It is of note that affinities of the *cis*-amide equivalents **16** and **17** for PEPT1 were more than 10 times weaker than those of *trans*-isomers. These data suggest that PEPT1 predominantly recognizes *trans*-amide conformations of dipeptides. This is in good accordance with the previous report by Brandsch et al., in which PEPT1 recognized *trans*-conformation of Ala-ψ[CS−N]-Pro.[19] Conformationally flexible analogues **26** and **27** retained moderate affinity in comparison with *cis*-amide equivalents. Presumably, analogues **26** and **27** could exist as *trans*-amide-like conformers, which were favorable for the interaction with PEPT1, due to their flexibility. Contrary to our expectation, an increase of affinity by the introduction of fluoroalkene unit was not observed (**24** vs **25**). Further investigation is required for verification of the effect of fluorine as a carbonyl oxygen mimic.

Table 1. K_i Values of Phe-Gly and Various Isosteres Based on Inhibition of [^{3}H]Gly-Sar Uptake by PEPT1 in Caco-2 Cell

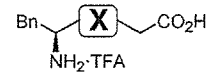

compd	X	K_i (mM)
Phe-Gly	−CO-NH−	0.205
16	−ψ[(*Z*)-CH=CH]−	>10.0
17	−ψ[(*E*)-CF=CH]−	>10.0
24	−ψ[(*E*)-CH=CH]−	0.853
25	−ψ[(*Z*)-CF=CH]−	1.34
26	−ψ[CH_2-CH_2]−	2.17
27	−ψ[CF_2-CH_2]−	1.67

In conclusion, we presented a novel unambiguous synthetic route for the syntheses of (*Z*)-alkene and (*E*)-fluoroalkene dipeptide isosteres as *cis*-amide bond mimetics via organocopper-mediated reduction of γ-acetoxy- or γ,γ-difluoro-α,β-unsaturated δ-lactams. We also carried out comparative studies of affinities for peptide transpoter PEPT1 between the *cis*-amide mimetics and the corresponding *trans*-amide isosteres, and found that peptide transporter PEPT1 predominantly recognizes *trans*-amide bond conformations in dipeptides. Synthetic studies on various α-substituted (*E*)-fluoroalkene isosteres and further structure−activity-relationship studies on dipeptide mimetics for PEPT1 are currently proceeding.

Acknowledgment. We thank Dr. Terrence R. Burke, Jr., NCI, NIH, for proofreading this manuscript. This research was supported in part by 21st Century COE Program "Knowledge Information Infrastructure for Genome Science", a Grant-in-Aid for Scientific Research from the Ministry of Education, Culture, Sports, Science and Technology, Japan, the Japan Society for the Promotion of Science (JSPS), and the Japan Health Science Foundation. A.N. is grateful for Research Fellowships from the JSPS for Young Scientists.

Supporting Information Available: Synthesis of compounds **24**−**27**. Experimental procedures and spectral data. This material is available free of charge via the Internet at http://pubs.acs.org.

OL052781K

(17) In ^{1}H NMR experiments, α-protons (position-3) of 3,6-*trans* isomers such as **18** or *trans*-**22** appeared upfield from the corrresponding α-protons of 3,6-*cis* isomeres. See ref 9.

(18) (a) Våbenø, J.; Lejon, T.; Nielsen, C. U.; Steffansen, B.; Chen, W.; Ouyang, H.; Borchardt, R. T.; Luthman, K. *J. Med. Chem.* **2004**, *47*, 1060. (b) Våbenø, J.; Nielsen, C. U.; Ingebrigtsen, T.; Lejon, T.; Steffansen, B.; Luthman, K. *J. Med. Chem.* **2004**, *47*, 4755. (c) Terada, T.; Inui, K. *Curr. Drug Metab.* **2004**, *5*, 85. (d) Biegel, A.; Gebauer, S.; Hartrodt, B.; Brandsh, M.; Neubert, K.; Thondorf, I. *J. Med. Chem.* **2005**, *48*, 4410.

(19) Brandsh, M.; Thunecke, F.; Küllertz, G.; Schutkowski, M.; Fischer, G.; Neubert, K. *J. Biol. Chem.* **1998**, *273*, 3861.

Efficient intervention of growth and infiltration of primary adult T-cell leukemia cells by an HIV protease inhibitor, ritonavir

M. Zahidunnabi Dewan, Jun-nosuke Uchihara, Kazuo Terashima, Mitsuo Honda, Tetsutaro Sata, Mamoru Ito, Nobutaka Fujii, Kimiharu Uozumi, Kunihiro Tsukasaki, Masao Tomonaga, Yoko Kubuki, Akihiko Okayama, Masakazu Toi, Naoki Mori, and Naoki Yamamoto

Adult T-cell leukemia (ATL), an aggressive malignancy of CD4+ T cells associated with human T-cell leukemia virus type I (HTLV-I) infection, carries a very poor prognosis because of the resistance of leukemic cells to any conventional regimen, including chemotherapy. We examined the effect of ritonavir, an HIV protease inhibitor, on HTLV-I–infected T-cell lines and primary ATL cells and found that it induced apoptosis and inhibited transcriptional activation of NF-κB in these cells. Furthermore, ritonavir inhibited expression of Bcl-x_L, survivin, c-Myc, and cyclin D2, the targets of NF-κB. In nonobese diabetic/severe combined immunodeficient (NOD/SCID)/γc^{null} (NOG) mice, ritonavir very efficiently prevented tumor growth and leukemic infiltration in various organs of NOG mice at the same dose used for treatment of patients with AIDS. Our data indicate that ritonavir has potent anti–NF-κB and antitumor effects and might be clinically applicable for treatment of ATL. These results would provide a new concept and novel platform for new drug development of leukemia and solid cancer as well. (Blood. 2006;107:716-724)

Introduction

Human T-cell leukemia virus type I (HTLV-I) is the causative agent of an aggressive form of CD4+ T-cell leukemia designated adult T-cell leukemia (ATL).[1-3] ATL was first identified in Japan in 1977.[4,5] Common findings for patients with ATL include enlargement of peripheral lymph nodes, hepatomegaly, splenomegaly, hypercalcemia, and skin lesions. At present, there is no accepted curative therapy for ATL, and patients progress to death with a median survival duration of 13 months in aggressive ATL.[6] ATL has a poor prognosis mainly because of its resistance to conventional as well as high-dose chemotherapy.

ATL develops after a long period of latent infection. This long latency suggests that multiple genetic events, which accumulate in HTLV-I–infected cells, are involved in the development of ATL. However, the precise molecular mechanism of leukemogenesis and the development of ATL after HTLV-I infection are not fully elucidated. A unique viral gene *Tax* is considered to play a central role in HTLV-I–induced transformation, which is responsible for transactivation of the HTLV-I long terminal repeat,[7,8] as well as numerous cellular genes involved in T-cell activation and growth, such as those encoding IL-2,[9] and the α-chain of IL-2 receptor (IL-2Rα) (CD25, Tac).[10,11] Induction of many cellular genes by Tax is mediated through the transcription factor NF-κB. The malignant cells associated with all phases of ATL express very high levels of IL-2Rα[12-14] without expressing a significant amount of Tax.

HTLV-I–infected cell lines derived from a leukemic cell clone and primary ATL cells failed to express significant amounts of Tax and other viral proteins, suggesting that the expression of viral proteins is not always necessary for leukemic proliferation at the late stage of the disease. However, HTLV-I–infected cell lines and leukemic cells from patients with ATL display constitutive NF-κB binding activity and increased degradation of a specific inhibitor, IκBα.[15] In resting cells, NF-κB is sequestered as an inactive precursor by association with inhibitory IκBs in the cytoplasm. On stimulation, IκBs are rapidly phosphorylated, ubiquitinated, and degraded by a proteasome-dependent pathway, allowing active NF-κB to translocate into the nucleus where it can activate the expression of a number of genes.[16] NF-κB activation has been connected with multiple processes of oncogenesis, including control of apoptosis, cell cycle, differentiation, and cell migration[16]; therefore, inhibition of NF-κB was suggested to be a useful

From the Department of Molecular Virology, Graduate School of Medicine, Tokyo Medical and Dental University, Tokyo, Japan; the AIDS Research Center, National Institute of Infectious Diseases, Tokyo, Japan; the Division of Molecular Virology and Oncology, Graduate School of Medicine, University of the Ryukyus, Okinawa, Japan; the Department of Pathology, National Institute of Infectious Diseases, Tokyo, Japan; the Central Institute for Experimental Animals, Kanagawa, Japan; the Department of Bioorganic Medical Chemistry, Graduate School of Pharmaceutical Sciences, Kyoto University, Kyoto, Japan; the Department of Epidemiology and Preventive Medicine, Kagoshima University Graduate School of Medical and Dental Sciences, Kagoshima, Japan; the Department of Hematology, Molecular Medicine Unit, Atomic Bomb Disease Institute, Nagasaki University Graduate School of Biomedical Sciences, Nagasaki, Japan; the Second Department of Internal Medicine, Miyazaki Medical College, University of Miyazaki, Miyazaki, Japan; the Department of Laboratory Medicine, Miyazaki Medical College, University of Miyazaki, Miyazaki, Japan; and the Division of Clinical Trials and Research, Breast Cancer Research and Treatment Program, Tokyo Metropolitan Komagome Hospital, Tokyo Medical Center for Cancer and Infectious Disease, Tokyo, Japan.

Submitted February 23, 2005; accepted September 1, 2005. Prepublished online as *Blood* First Edition Paper, September 20, 2005; DOI 10.1182/blood-2005-02-0735.

Supported by grants from the Ministry of Education, Science, and Culture; the Ministry of Health, Labor, and Welfare; and Human Health Science of Japan.

M.Z.D. and J.U. contributed equally to the study.

Reprints: Naoki Yamamoto, Department of Molecular Virology, Graduate School of Medicine, Tokyo Medical and Dental University, 1-5-45 Yushima, Bunkyo-ku, Tokyo 113-8519, Japan; e-mail: yamamoto.mmb@tmd.ac.jp; and Naoki Mori, Division of Molecular Virology and Oncology, Graduate School of Medicine, University of the Ryukyus, 207 Uehara, Nishihara, Okinawa 903-0215, Japan; e-mail: n-mori@med.u-ryukyu.ac.jp.

The publication costs of this article were defrayed in part by page charge payment. Therefore, and solely to indicate this fact, this article is hereby marked "advertisement" in accordance with 18 U.S.C. section 1734.

strategy for cancer therapy.[17-20] Despite the diversity in clinical manifestations of ATL, strong and constitutive NF-κB activation was reported to be a unique and common characteristic of ATL cells.[15] Thus, the indispensability of NF-κB for the maintenance of the malignant phenotype of HTLV-I provides a possible molecular target for ATL therapy.[21-24]

Ritonavir, a human immunodeficiency virus type 1 (HIV-1) protease inhibitor (PI), has been successfully used in clinical treatments of HIV infection, with patients exhibiting a marked decrease in HIV viral load and a subsequent increase in $CD4^+$ T-cell counts.[25-28] Evidence of other effects by ritonavir on cellular proteases, such as the cysteine proteases cathepsin D and E, was presented in the drug's original description, albeit at concentrations greater than 500-fold above the concentration required for inhibition of HIV protease.[29] PIs have also been shown to directly affect cell metabolism, interfere with host or fungal proteases, and block T-cell activation and dendritic cell function.[30,31] Recently, ritonavir has been shown to inhibit the chymotrypsin-like activity of the 20S proteasome, and it activates the chymotrypsin-like activity of the 26S proteasome conversely.[30,32,33] Ritonavir also has been reported to inhibit the transactivation of NF-κB induced by activators such as TNFα, HIV-1 Tat protein, and the human herpesvirus 8 protein ORF74. It is possible that inhibition of NF-κB activation by ritonavir is linked to additional pathways other than inhibition of proteasome.[34] PIs also have been shown to have direct antiangiogenic and antitumor activity[34,35]

In this study, we investigated the antitumor effects of ritonavir on HTLV-I–infected cell lines and primary ATL cells. We found that ritonavir decreases NF-κB activity linked to the inhibition of IκBα phosphorylation and induces apoptosis of these cells. In addition, we established preclinical models to evaluate the efficacy of anti-ATL and anti–NF-κB therapies. In the ATL model, ritonavir potently inhibited the growth and infiltration of leukemic cells from patients at concentrations used for treatment of patients with AIDS.

Materials and methods

Cell lines

The T-cell leukemia cell line Jurkat, HTLV-I–infected T-cell lines MT-2,[36] MT-4,[37] C5/MJ,[38] SLB-1,[39] HUT-102,[2] MT-1,[40] and ED-40515(−),[41] and bcr-abl$^+$ leukemic cell line K562 were cultured in RPMI 1640 medium supplemented with 2% heat-inactivated fetal bovine serum (JRH Biosciences, Lenexa, KS), 100 U/mL penicillin, and 10 μg/mL streptomycin. MT-2, MT-4, C5/MJ, and SLB-1 are HTLV-I–transformed T-cell lines. MT-1 and ED-40515(−) are T-cell lines of leukemic cell origin established from patients with ATL. The clonal origin of HUT-102 is unclear.

Human specimens

Leukemic cells from 38 patients (8 patient samples for in vitro studies, 20 for establishment of ATL model, 10 for in vivo ritonavir studies) diagnosed as either acute type or chronic type were used in this study. The diagnosis of ATL was based on clinical features, hematologic findings, and the presence of anti–HTLV-I antibodies in the sera. Baseline characteristics for the patients who entered the study are shown in Table 1. Monoclonal HTLV-I provirus integration into the DNA of leukemia cells was confirmed by Southern blot hybridization in all cases (data not shown). All samples were collected after obtaining informed consent from patients. Peripheral blood mononuclear cells (PBMCs) from healthy volunteers and patients with ATL were purified by Ficoll-Hypaque gradient centrifugation (Amersham Biosciences, Uppsala, Sweden) and washed with RPMI 1640.

Growth inhibition assay

The effect of ritonavir on cell growth was assayed by the WST-8 method as described previously.[42] The WST-8 Cell Counting Kit was obtained from Wako Chemicals (Osaka, Japan). Briefly, 2×10^5 cells were incubated in a 96-well microculture plate in the absence or presence of various concentrations of ritonavir. After 72 hours of culture, 10 μL WST-8 solution was added, and the cells were incubated for another 2 hours. The number of surviving cells was measured with a microplate reader at a reference wavelength of 655 nm and test wavelength of 450 nm. Cell viability was determined as the percentage of the control (ie, absence of ritonavir).

Assay for apoptosis

Quantification of apoptosis was performed by immunostaining cells with Apo2.7, which specifically detects the 38-kDa mitochondrial membrane antigen 7A6 present only on the mitochondrial membrane of apoptotic cells, and so can be used as an early apoptotic marker in cells.[43,44] Cells cultured for 72 hours in the absence or presence of various concentrations of ritonavir were labeled with the Apo2.7-phycoerythrin–conjugated monoclonal antibody (Beckman-Coulter/Immunotech, Miami, Florida) or mouse IgG1 isotype control (Beckman-Coulter/Immunotech) and subsequently analyzed by flow cytometry.

EMSA

Cells were placed in culture at 1×10^6 cells/mL (cell line) or 5×10^6 cells/mL (PBMCs) and examined for inhibition of NF-κB after exposure to ritonavir. Nuclear proteins were extracted, and NF-κB binding activities to κB element were examined by electrophoretic mobility shift assay (EMSA) as described previously.[15] In brief, 5 μg nuclear extracts were preincubated in a binding buffer containing 1 μg poly(dI:dC) (Amersham Biosciences), followed by addition of ^{32}P-labeled oligonucleotide probe containing NF-κB element (5×10^4 cpm). These mixtures were incubated for 15 minutes at room temperature. The DNA-protein complexes were separated on a 4% polyacrylamide gel and visualized by autoradiography. To examine the specificity of the NF-κB element probe, unlabeled competitor oligonucleotides were preincubated with nuclear extracts for 15 minutes before incubation with probes. The probe or competitors used were prepared by annealing the sense and antisense synthetic oligonucleotides as follows: a typical NF-κB element from the *IL2RA* gene, 5′-gatcCGGCAGGG-GAATCTCCCTCTC-3′; and AP-1 element of the *IL8* gene, 5′-gatcGTGAT-GACTCAGGTT-3′. Underlined sequences represent the NF-κB or AP-1 binding site. To identify NF-κB proteins in the DNA protein complex revealed by EMSA, we used antibodies specific for various NF-κB proteins, including p65, p50, c-Rel, and p52 (Santa Cruz Biotechnology, Santa Cruz, CA), to elicit a supershift DNA protein complex formation. These antibodies were incubated with the nuclear extracts for 45 minutes at room temperature before incubation with radiolabeled probes.

Western blot analysis

Treated cells were solubilized at 4°C in lysis buffer containing 62.5 mM Tris-HCl (pH 6.8), 2% SDS, 10% glycerol, 6% 2-mercaptoethanol, and 0.01% bromophenol blue. Samples were subjected to electrophoresis on SDS-polyacrylamide gels followed by transfer to a polyvinylidene difluoride membrane and probing with the following specific antibodies: polyclonal antibodies against IκBα, cIAP2, survivin, cyclin D2 (Santa Cruz Biotechnology), Bcl-X_L (Transduction Laboratories, San Jose, CA), and c-Myc (NeoMarkers, Fremont, CA) and monoclonal antibodies against phospho-IκBα, hyperphosphorylated form of pRb (Cell Signaling Technology, Beverly, MA), Bcl-2, and actin (NeoMarkers). The protein bands recognized by the antibodies were visualized using the enhanced chemiluminescence system (Amersham, Piscataway, NJ).

Plasmids and transfection

Reporter plasmid κB-LUC (kindly provided by J. Fujisawa, Kansai Medical University, Osaka, Japan) is a luciferase expression plasmid controlled by 5 tandem repeats of a NF-κB binding site from the *IL2RA*

Table 1. Clinical characteristics of patients

Patient	Age, y/sex	Diagnosis	WBC count, cells × 10^9/L	Lymphocytes, %	Atypical cells, %	Treatment status
1	54/M	Acute	192.80	65.0	91.0	Untreated
2	77/F	Acute	186.0	41.0	70.0	Untreated
3	67/F	Chronic	10.40	38.0	89.0	Treated
4	58/M	Acute	67.30	71.0	80.0	Treated
5	71/M	Acute	19.70	51.0	61.0	Treated
6	66/F	Chronic	29.40	49.0	75.0	Untreated
7	48/F	Chronic	9.40	29.0	55.0	Untreated
8	69/F	Acute	53.80	44.0	95.0	Treated
9	58/M	Chronic	11.30	59.0	70.0	Treated
10	60/M	Chronic	9.12	61.0	80.0	Treated
11	65/F	Acute	29.40	25.0	60.0	Untreated
12	49/F	Chronic	15.10	48.0	75.0	Treated
13	57/M	Chronic	10.00	50.0	57.0	Treated
14	72/F	Acute	39.00	70.0	80.0	Treated
15	79/F	Chronic	10.10	47.0	27.0	Untreated
16	68/F	Acute	7.00	86.0	86.0	Treated
17	59/F	Chronic	8.99	74.5	40.0	Treated
18	70/M	Acute	31.60	71.7	68.0	Treated
19	49/M	Acute	5.00	19.5	78.0	Treated
20	44/M	Chronic	36.40	33.0	43.0	Untreated
21	65/F	Chronic	14.70	76.0	22.0	Untreated
22	63/F	Acute	12.40	71.0	82.0	Untreated
23	56/F	Chronic	7.20	46.0	15.0	Treated
24	78/F	Acute	94.50	63.3	49.0	Treated
25	62/F	Acute	10.10	53.0	27.0	Untreated
26	66/M	Chronic	38.10	63.0	39.0	Treated
26	39/F	Chronic	18.50	16.0	57.0	Untreated
28	48/F	Acute	53.50	39.0	64.0	Untreated
29	75/F	Acute	15.00	72.0	65.0	Untreated
30	84/F	Acute	14.40	69.0	61.0	Treated
31	73/M	Chronic	7.80	59.0	47.0	Untreated
32	43/F	Chronic	18.60	63.0	43.0	Untreated
33	54/F	Acute	69.00	49.0	50.0	Untreated
34	66/F	Acute	10.20	38.0	51.0	Untreated
35	73/F	Chronic	15.70	58.0	39.0	Untreated
36	63/F	Acute	32.90	71.0	95.0	Treated
37	44/F	Chronic	22.60	51.0	45.0	Untreated
38	68/M	Acute	30.00	79.0	81.0	Untreated

WBC indicates white blood cells.

gene. Reporter plasmid AP-1–LUC (kindly provided by N. Mukaida, Kanazawa University, Kanazawa, Japan) is a luciferase expression plasmid controlled by 2 copies of the AP-1 binding site from the IL-8 promoter. The expression plasmid for HTLV-I Tax has been described previously.[45] Transient transfections were performed in Jurkat and HUT-102 cells by electroporation using 5×10^6 cells and reporter and effecter plasmids. To normalize transfection efficiencies, a thymidine kinase (TK) promoter-driven Renilla luciferase plasmid (phRL-TK; Promega, Madison, WI) was cotransfected as an internal control plasmid. Then, 16 hours after transfection, ritonavir was added to the cultures at various concentrations, and cells were further cultured for 24 hours for assay of luciferase activity. Transfected cells were collected by centrifugation, washed with phosphate-buffer saline (PBS), and lysed in reporter lysis buffer (Promega). Lysates were assayed for reporter gene activity with the dual-luciferase reporter assay system (Promega).

Inoculation of ATL cells and collection of samples

NOG mice were obtained from the Central Institute for Experimental Animals (Kawasaki, Japan). All mice were maintained under specific pathogen-free conditions in the Animal Center of National Institute of Infectious Diseases (Tokyo, Japan). The Ethical Review Committee of the Institute approved the experimental protocol. Mice were anesthetized with ether, and cells were inoculated either intraperitoneally in abdominal region or subcutaneously in the postauricular region of NOG mice without injection of human recombinant IL-2 at a dose of 1 to 2×10^7 cells per mouse. All mice were killed 30 or 60 days after inoculation with primary ATL cells. Blood was collected from the tail to make a smear, as well as from the heart with heparinized syringes. PBMCs and splenocytes were isolated by density gradient concentration with Ficoll-Hypaque. Blood smear slides were fixed in methyl alcohol for May-Grunwald and Giemsa staining. PBMCs and splenocytes were stored at −80°C for further experiments. Tissues and various organs of mice were collected and fixed with Streck Tissue Fixative, then processed to paraffin wax-embedded sections for staining with hematoxylin and eosin (HE) and immunostaining.

Treatment of ATL mice with ritonavir

Ritonavir was obtained from Abbott Labs, North Chicago, IL. Primary ATL cells (2×10^7) from 10 patients were inoculated subcutaneously in the postauricular region of NOG mice. One day after inoculation of ATL cells, mice were treated with either RPMI 1640 (control mice) or drug (ritonavir 30 mg/kg/d) intraperitoneally daily for 30 days followed by observation for another 30 days without treatment. ATL cell growth and progression were monitored by observation of physical condition of mice during a 2-month follow-up period.

Immunohistochemistry

Paraffinized cryosections of various organs were deparaffinized and hydrated in xylenes or clearing agents and graded alcohol series, then rinsed for 5 minutes in water. Deparaffinized samples were incubated with 0.025% trypsin/PBS for 30 minutes followed by washing, and then incubated with 0.3% methanol for 30 minutes at room temperature and washed 2 times with PBS. Immunostaining was done as described previously[46] using Vector MOM immunodetection kit (Vector Labs, Burlingame CA) for ATL cells with a 1:500 dilution of primary mouse monoclonal antibody specific for human CD4 and CD25 (Dako, Caterpillar, CA). This was followed by washing in PBS and incubation with a secondary antibody MOM biotinylated anti–mouse IgG, after which cells were again washed in PBS and incubated with VECTASTAIN *Elite* ABC for 20 minutes at room temperature. Positive staining was visualized after incubation of these samples with a mixture of 0.05% 3,3′-diaminobenzidine tetrahydrochloride in 50 mM Tris-HCl buffer and 0.01% hydrogen peroxide for 5 minutes. The samples were counterstained with hematoxylin for 2 minutes, hydrated completely, cleaned in xylene, and then mounted. Photographs were taken by light microscopy (BX41, Olympus, Tokyo, Japan) using UplanF1 lenses (DP70, Olympus; magnification ×40).

Results

Ritonavir reduces cell growth and induces apoptosis of HTLV-I–infected cell lines and primary ATL cells

Ritonavir was examined for its effect on proliferation of HTLV-I–infected cell lines (Figure 1A). Ritonavir effectively inhibited the proliferation of HTLV-I–infected cell lines as measured by WST-8 on the third day of culture in a dose-dependent manner, but not that of K562 cells. Further experiments using Apo2.7 showed that ritonavir caused apoptosis of HTLV-I–infected cell lines in a dose-dependent manner, but not that of K562 cells (Figure 1B-C). In addition, we explored the anti-ATL effect of ritonavir on freshly isolated ATL cells from patients. In all ATL cases, ritonavir reduced the survival of ATL cells in a dose-dependent manner (Figure 1D). Ritonavir also caused apoptosis of ATL cells (Figure 1E). In contrast, ritonavir hardly affected the survival of peripheral blood mononuclear cells (PBMCs) from 3 healthy volunteers as measured by WST-8 (Figure 1D).

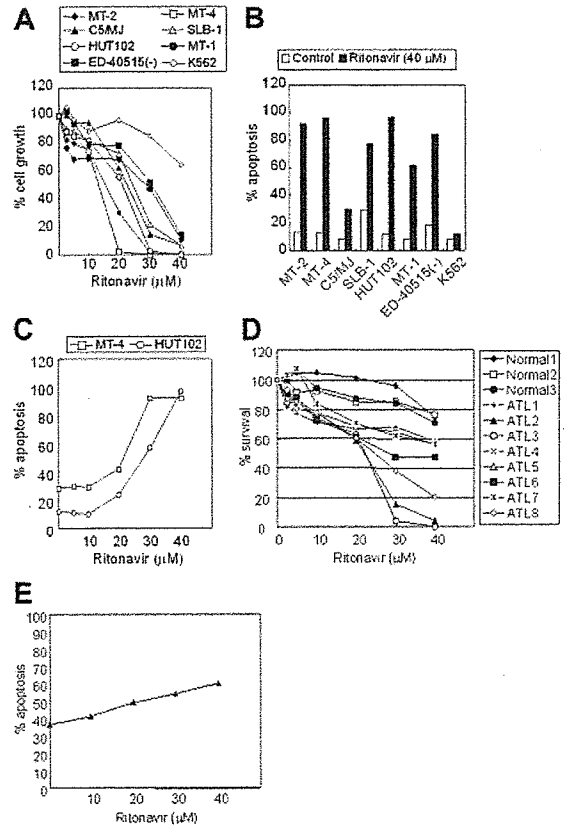

Figure 1. Effect of ritonavir on the growth and induction of apoptosis of HTLV-I–infected cell lines and freshly isolated ATL cells. (A) Dose-response effect of ritonavir on the growth of HTLV-I–infected cell lines. Cells (10^5/mL) were cultured for 72 hours in the presence of various concentrations (2.5-40 μM) of ritonavir. Cell growth was assessed by the water-soluble tetrazolium (WST)-8 method and is expressed as a percentage of control (untreated cells) and represents the mean of triplicate cultures. (B) Effect of ritonavir on induction of apoptosis of HTLV-I–infected cell lines. Cells were cultured for 72 hours with ritonavir (40 μM), and apoptosis was measured by Apo2.7 immunostaining. Data represent the mean percentages of apoptotic cells from both untreated (□) and ritonavir-treated (■) cells. (C) Dose-response effect of ritonavir on induction of apoptosis of MT-4 and HUT-102 cells. (D) Dose-response effect of ritonavir on the cell viability of freshly isolated ATL cells. Cells (10^6/mL) were cultured for 72 hours in the presence of various concentrations (2.5-40 μM) of ritonavir. (E) Dose-response effect of ritonavir on induction of apoptosis of ATL cells.

Ritonavir suppresses constitutive NF-κB expressed by HTLV-I–infected cell lines and primary ATL cells

To examine the effect of ritonavir on NF-κB DNA binding, electrophoretic mobility shift assay (EMSA) was performed. We first examined the minimum duration of exposure to ritonavir required for suppression of NF-κB. For this, HUT-102 cells were incubated with 40 μM ritonavir for different periods of time, and nuclear extracts were prepared and examined for NF-κB by EMSA. Down-regulation of NF-κB occurred at 24 hours in HUT-102 cells. However, no change in binding activity of AP-1 was observed (Figure 2A). The observed protein/DNA binding was specific for NF-κB, because the binding was effectively competed and abrogated by excess unlabeled NF-κB oligonucleotide but not by AP-1 (Figure 2C). The NF-κB complex contained p50, p65, and c-Rel (Figure 2C). Forty micromolar concentration of ritonavir was sufficient to suppress constitutive NF-κB activation in residual HTLV-I–infected T-cell lines (data not shown). It should be noted that K562 cells did not show constitutive NF-κB activation (data not shown). We also found a concentration-dependent inhibitory effect of ritonavir on the constitutive increase of NF-κB DNA binding activity (Figure 2B). Twenty micromolar concentration of ritonavir caused only a partial inhibition of NF-κB/DNA binding, whereas strong inhibition was observed at 30 and 40 μM in HUT-102 cells. However, AP-1 binding was not inhibited. This inhibition coincided with an accumulation of unphosphorylated IκBα and a decrease of the slower-migrating form of phosphorylated IκBα, a prerequisite for its subsequent degradation (Figure 2D, top). Thirty micromolar concentration of ritonavir caused only a partial decrease of the slower-migrating form of phosphorylated IκBα, whereas significant decrease of the slower-migrating form of phosphorylated IκBα and an accumulation of unphosphorylated IκBα were observed at 40 μM. We determined the alteration of phosphorylation of IκBα using antibody against phosphospecific IκBα. Results in Figure 2D (middle) show that 40 μM ritonavir decreased the phosphorylated IκBα content. We also determined whether the same results were obtained in primary ex vivo ATL specimens. As shown in Figure 2E, the amount of NF-κB that translocates to the nucleus is also decreased, as determined by EMSA. Twenty micromolar concentration of ritonavir caused only a partial inhibition of NF-κB/DNA binding, whereas strong inhibition was observed at 30 μM in primary ATL cells from acute

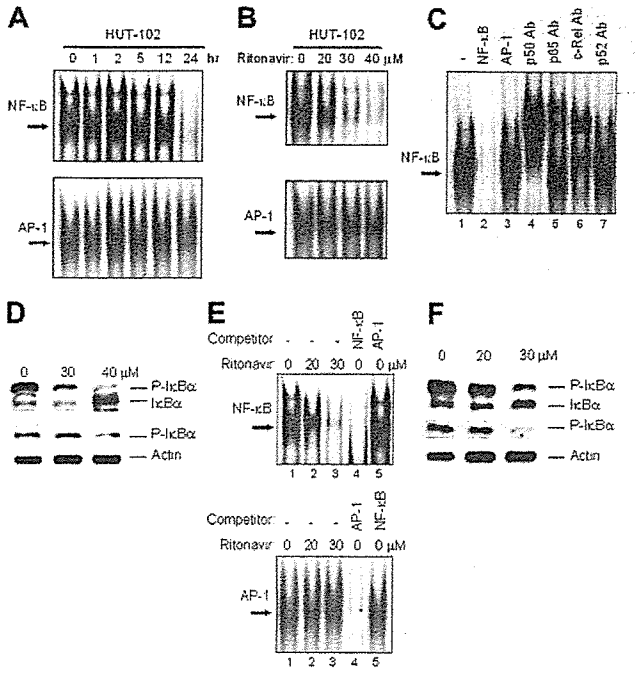

Figure 2. Ritonavir inhibits constitutive NF-κB activation. (A) HUT-102 cells treated with ritonavir (40 μM) for the indicated time were evaluated for NF-κB and AP-1 activation. (B) HUT-102 cells treated with the indicated concentration of ritonavir for 24 hours were evaluated for NF-κB and AP-1 activation. (C) Cold competition using 100-fold molar excess of unlabeled NF-κB and AP-1 oligonucleotides (lanes 2 and 3) demonstrated the specificity of the protein/DNA binding complexes. Specificity of NF-κB binding was also determined by using antibodies to the NF-κB components p50, p65, c-Rel, and p52, resulting in supershift (lanes 4-7). (D) HUT-102 cells were treated with the indicated concentration of ritonavir for 24 hours, and cell lysates were immunoblotted for IκBα (top) and phospho-IκBα (middle). Actin immunoblots confirm that similar amounts of cell extracts were analyzed (bottom). (E) Primary acute-type ATL cells treated with concentrations of ritonavir as indicated for 24 hours were evaluated for NF-κB and AP-1 activation. Where indicated, 100-fold excess amounts of competitor oligonucleotides were added to the reaction mixture (lanes 4 and 5). (F) The bands of phosphorylated IκBα were down-regulated by ritonavir treatment. Detection of actin expression was used as an internal control.

type. However, AP-1 binding was not inhibited. Ritonavir abolished proximal signaling events leading to IκBα phosphorylation (Figure 2F). Twenty micromolar concentration of ritonavir caused only a partial decrease of the slower-migrating form of phosphorylated IκBα, whereas significant decrease of the slower-migrating form of phosphorylated IκBα and an accumulation of unphosphorylated IκBα were observed at 30 μM (top). Thirty micromolar concentration of ritonavir abolished the phosphorylated IκBα content (middle). We obtained similar results using another acute-type ATL cells (data not shown).

Ritonavir represses Tax-induced and constitutive transcriptional activity of NF-κB

We examined whether ritonavir inhibits the transcriptional activity of NF-κB. First, we tested the effect of ritonavir on Tax-induced NF-κB transcriptional activity in Jurkat cells (HTLV-I–uninfected cell line) transfected with Tax expression plasmid. Ritonavir caused only a partial inhibition of proliferation in Jurkat cells cultured for 24 hours even at the highest dose. Tax-induced NF-κB transcriptional activation was suppressed by ritonavir in a dose-dependent manner (Figure 3A). Next, we determined the effect of ritonavir on constitutively activated NF-κB and AP-1 transcriptional activity in an HTLV-I–infected cell line HUT-102. Ritonavir inhibited the constitutively activated transcriptional activity of NF-κB in a dose-dependent manner, but not that of AP-1 (Figure 3B). Twenty micromolar concentration of ritonavir caused only a partial inhibition of NF-κB/DNA binding (Figure 2B), whereas strong inhibition of NF-κB transcriptional activity was observed at the concentration less than 20 μM. This discrepancy might derive from differences in sensitivity between these 2 assays. These results indicate that ritonavir inhibits both Tax-induced and constitutive NF-κB transcriptional activity.

Ritonavir down-regulates the expression of NF-κB–regulated gene products

The antiproliferative and proapoptotic effects of ritonavir were explored by examining the level of intracellular regulators of cell cycle and apoptosis after exposure to ritonavir (Figure 3C). Ritonavir down-regulated levels of Bcl-X_L, survivin, cIAP2, c-Myc, cyclin D2, regulated by NF-κB,[47-51] and the phosphorylated form of pRb in HUT-102 cells cultured with 40 μM ritonavir for 72 hours. Thirty micromolar concentration of ritonavir caused only a partial down-regulation of Bcl-X_L and the phosphorylated form of pRb, whereas significant down-regulation of survivin was observed in HUT-102 cells cultured for 72 hours, suggesting that NF-κB–regulated genes have the differential sensitivity to ritonavir. However, ritonavir did not modulate levels of Bcl-2 and Tax proteins in these cells (Figure 3C; data not shown). We also explored the effect of ritonavir on NF-κB–regulated gene products in ATL cells freshly isolated from an acute-type patient. As shown in Figure 3D, Bcl-X_L, survivin, cyclin D2, and c-Myc, but not Bcl-2, showed a decline. Thus, expression of NF-κB regulated genes, the induction of which are involved in antiapoptosis (Bcl-X_L, survivin, and cIAP2) and cell cycle (cyclin D2 and c-Myc), apparently had been down-regulated in the presence of ritonavir. We obtained a similar result using other acute-type ATL

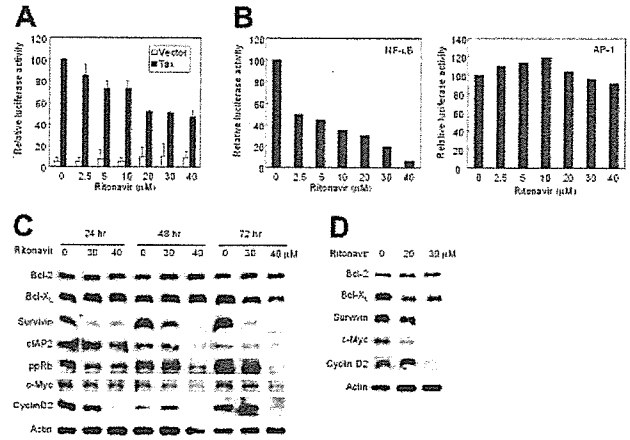

Figure 3. Ritonavir inhibits NF-κB transcriptional activation and expression of apoptosis- and cell-cycle–associated proteins. (A) Ritonavir inhibits Tax-induced NF-κB transcriptional activation. κB-LUC was transfected into Jurkat cells with Tax-expressing plasmid (■) or empty vector (□). After transfection, cells were treated with increasing concentrations of ritonavir. Luciferase activity is expressed relative to the basal level measured in cells transfected with the reporter plasmid and Tax-expressing plasmid without further treatment, which was defined as 100. Data represent the mean + SD from 3 independent experiments. (B) Ritonavir inhibits constitutive active NF-κB transcriptional activity in HUT-102 cells. κB-LUC and AP-1–LUC were transfected into HUT-102 cells. After transfection, cells were treated as in panel A. Luciferase activity was normalized, based on the Renilla luciferase activity from phRL-TK. Relative luciferase activity is expressed relative to the basal level measured in cells transfected with the reporter plasmid without further treatment, which was defined as 100. (C-D) Western blot analyses. HUT-102 cells (C) and primary acute-type ATL cells (D) were cultured with the indicated concentration of ritonavir for 24 to 72 hours (HUT-102 cells) and 24 hours (ATL cells). Cells were harvested and subjected to Western blot analysis. The polyvinylidene fluoride membrane was sequentially probed with indicated antibodies.

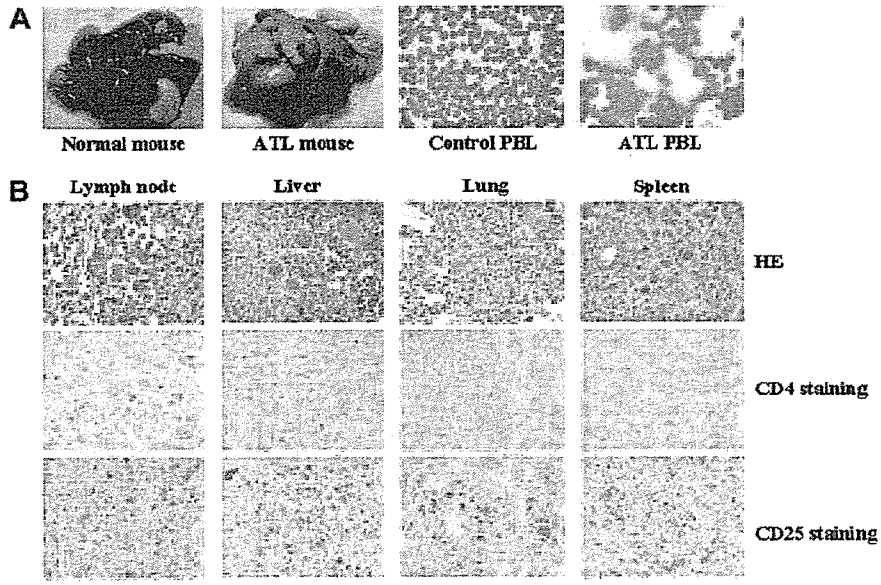

Figure 4. Successful engraftment and massive infiltration of primary ATL cells into various organs of NOG mice inoculated with PBMCs from patients with ATL. (A) Photographs of whole organs of normal and ATL cell–challenged mice with enlarged spleen, liver, and lungs (left 2 panels). Right 2 panels show May-Grunwald and Giemsa staining of PBMCs collected from normal and ATL cell–challenged mice, 2 months after inoculation of ATL cells, respectively. (B) HE (top) and immunohistochemical staining of various organs of NOG mice inoculated with ATL cells. Immunohistochemical staining using anti-CD4 (middle) and anti-CD25 (bottom) was conducted on various organs of mice tissues 2 months after inoculation of ATL cells. Magnification ×40.

cells (data not shown). Taken together these data suggest that constitutively high NF-κB activity in ATL cells is indispensable for their survival, and that specific inhibition of this activity by a clinically available drug results in the induction of apoptosis.

Establishment of a novel ATL model

PBMCs from patients with ATL were inoculated either intraperitoneally into the abdominal region or subcutaneously in the postauricular region of unconditional NOD/SCID/γc^{null} (NOG) mice. All mice developed clinical sign of near-death, such as piloerection, weight loss, and cachexia 6 to 8 weeks after inoculation of ATL cells in addition to the enlargement of lymph nodes, spleen, lungs, and liver, whereas no tumors were found in the postauricular region or abdominal cavity where primary ATL cells were inoculated (Figure 4A). There was no difference in respect to the successful engraftment of ATL cells inoculated either intraperitoneally or subcutaneously in NOG mice. Histologic analysis of ATL-bearing mice showed massive infiltration of leukemic cells in various organs of NOG mice that were efficiently expressing human CD4 and CD25 molecules (Figure 4B). A higher level of IL-2Rα (CD25) expression was observed on the surface of malignant cells associated with all stages of ATL[12-14] as well as ATL cells infiltrated into various organs of patients.[52,53] Thus, results from this model indicated successful engraftment and massive infiltration of primary ATL cells in various organs of NOG mice, like leukemia but without producing tumors at the sites of inoculation.

Ritonavir inhibits ATL cell growth and infiltration in NOG mice

To study the effect of ritonavir on ATL, we injected primary ATL cells (2×10^7) from 10 patients subcutaneously into the postauricular region of NOG mice. One day after inoculation, mice were treated with either RPMI-1640 (as control) or ritonavir (30 mg/kg/d) intraperitoneally daily for 30 days followed by observation for another 30 days without any treatment. ATL cell inoculation promoted the development of piloerection, weight loss, and cachexia, all of which are signs of near-death, in addition to the enlargement of lymph nodes, spleen, lungs, and liver in all control mice 2 months after inoculation (Figure 5A). In contrast, ritonavir-treated mice appeared to be healthy and had almost no enlargement of these organs (Figure 5A). Clinical evaluation of organ invasion 2 months after injection of primary ATL cells showed that ritonavir treatment inhibited their infiltration into lymph nodes, spleen, lungs, and liver (Figure 5B-D). Samples from 7 patients of 10 injected in mice treated with ritonavir presented substantial inhibition of organ invasion, and 2 (patients 5 and 7) showed partial inhibition, whereas one sample (patient 6) failed to do so (Table 2).

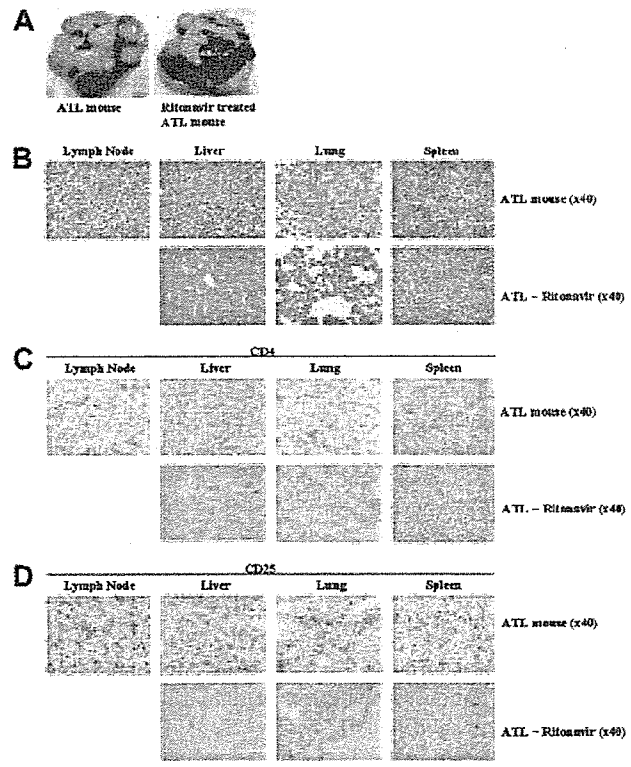

Figure 5. Effect of ritonavir on ATL cell growth and infiltration. (A) Mice were injected with ATL cells (2×10^7 cells) subcutaneously in the postauricular region. One day after inoculation, the mice were administered either RPMI 1640 or ritonavir (30 mg/kg/d) intraperitoneally every day for 30 days followed by observation for another month without therapy. Photographs of whole organs of RPMI 1640–treated ATL mice (left) and ritonavir-treated ATL mice (right) with enlarged spleen, liver, and lungs. (B-D) HE staining (B) and immunohistochemical staining using anti-CD4 (C) or anti-CD25 (D) in various organs of NOG mice 2 months after inoculation of ATL cells. Upper panels show various organs of mice treated with RPMI 1640, and lower panels represent various organs of mice treated with ritonavir. Magnification ×40.

Table 2. Effect of ritonavir on infiltration of ATL cells in various organs of SCID mice

Patient no. and treatment	Liver	Spleen	Lung	Lymph node
1				
Control	+++	+++	+++	+++
Ritonavir	++	+	+	NF
2				
Control	+++	+++	++	+++
Ritonavir	+	+	−	NF
3				
Control	+++	+++	+++	+++
Ritonavir	±	±	±	NF
4				
Control	+++	+++	+++	+++
Ritonavir	+	+	+	NF
5				
Control	+++	+++	+++	+++
Ritonavir	++	++	++	NF
6				
Control	+++	+++	+++	+++
Ritonavir	+++	++	+++	++
7				
Control	+++	+++	+++	+++
Ritonavir	++	+	++	NF
8				
Control	+++	+++	+++	+++
Ritonavir	±	±	±	NF
9				
Control	+++	+++	+++	++
Ritonavir	++	+	+	NF
10				
Control	+++	+++	++	+++
Ritonavir	+	+	+	NF

PBMCs from patients with ATL patients were inoculated subcutaneously into postauricular region of NOG mice, which were treated with ritonavir or RPMI-1640 as a control 1 day after inoculation for 1 month. Various organ infiltration was evaluated 2 months after inoculation.

NF indicates no formation of new lymph node; +++, massive; ++, marked; +, slight; ±, focally present or no infiltration; −, no infiltration.

In contrast, all control mice showed formation of new lymph nodes and infiltration with ATL cells into various organs (Figure 5B-D; Table 2). Organ infiltration of primary ATL cells was analyzed and evaluated by HE staining and immunostaining of CD4 and CD25. Together, these data indicate that ritonavir significantly inhibits ATL cell growth and infiltration in various organs of NOG mice (Figure 5).

Discussion

ATL is a malignancy of $CD4^+$ T-lymphocytes etiologically linked to a retrovirus, HTLV-I.[1-3] The malignant cells associated with all phases of ATL express very high levels of IL-2Rα (CD25).[12-14] The median survival duration of all patients with aggressive ATL was 13 months, and overall survival at 2 years was estimated to be 31.3%.[6] The various chemotherapies so far developed have not increased significantly the survival of patients with ATL. Given disappointing results using conventional chemotherapy, new approaches for the treatment of ATL are required. Previous reports have shown that primary ATL cells proliferate and infiltrate into various organs of SCID mice.[54-56] Our ATL model was consistent with others, but it represented more aggressive features about cell growth and infiltration in SCID mice. The tumor cells massively infiltrated into various organs in a manner similar to a leukemia-expressing T-cell marker CD4 and an activating marker CD25, especially into the spleen, lymph nodes, liver, and lungs of NOG mice. Our NOG ATL model presents many features 6 to 8 weeks after inoculation of ATL cells such as the clinical signs observed in patients with ATL. Two clinical types, acute and chronic, carry very different prognosis. However, no difference of cell growth, surface phenotype, and NF-κB activity is observed in primary leukemic cells from patients with acute- and chronic-type ATL. Therefore, the same characteristics of freshly isolated ATL cells with acute- and chronic-type were observed in NOG mice. Thus, it represents a novel model to evaluate tissue toxicity and the efficacy of therapeutic agents directed toward the treatment of ATL.

Constitutive NF-κB activation was demonstrated not only in HTLV-I–infected cell lines but also on fresh ATL cells regardless of Tax expression,[15] which could contribute to the drug-resistance of ATL cells through overexpression of Bcl-X_L.[51] We and others have previously reported that suppression of high NF-κB activity inhibited cell growth and induced apoptosis of HTLV-I–infected cell lines and primary ATL cells both in vitro and in vivo.[21-24] Recently, ritonavir has been shown to inhibit NF-κB activity induced by activators such as TNFα, Tat, and ORF74.[34] This led us to investigate whether this drug exhibits anti-ATL effects in vitro and in our preclinical murine ATL model. In the present study, we revealed that ritonavir treatment of HTLV-I–infected cell lines and ATL cells inhibited phosphorylation of IκBα, allowing suppression of NF-κB activity. Our results also suggest that inhibition of NF-κB activity by ritonavir reduced cell growth and induced apoptosis of these cells. This is consistent with down-modulation of NF-κB–regulated genes such as antiapoptotic (Bcl-X_L,[50,51] cIAP2,[57] and survivin[49]) and cell-cycle–related (cyclin D2[48] and c-Myc[47]) genes. We also examined the effect of ritonavir on the proliferation of an HTLV-I–negative T-cell line, Jurkat, in vitro. Exposure of ritonavir for 72 hours reduced the rate of proliferation (data not shown). Because ritonavir is suggested to affect proteasomal proteolysis,[33] it may effect a stabilization of p21, p27, and p53 proteins. Like proteasome inhibitors, ritonavir may also affect multiple pathways critical for survival of HTLV-I–positive and –negative malignant T cells. Additional experiments will be necessary to elucidate the mechanisms of anti-ATL activity.

In the therapy of HIV infection, the blood plasma ritonavir concentrations are between 5 and 15 μM,[58] but much higher maximal concentrations (up to 46 μM) have been determined in individual patients.[59] In the present study, we used the concentration of ritonavir for doing in vitro experiments from 0 to 40 μM and in vivo 30 mg/kg/d used for treatment of patients with AIDS. Our murine ATL model clearly indicates that 30 mg/kg/d of ritonavir significantly inhibits ATL cell growth and infiltration into various organs of NOG mice. The plasma exposure produced by this dose in mice is only approximately one half of the plasma exposure observed with the licensed dose of ritonavir in humans (600 mg twice daily). In our NOG ATL model, ritonavir at this treatment dosage is well tolerated without severe adverse effects observed in the mice during the treatment period. These data strongly suggest that the HIV PI, ritonavir, is a promising antitumor agent against ATL and could be used clinically for ATL regimens. Ritonavir exhibited anti-ATL activity against leukemic cells from patients

with acute- and chronic-type ATL in vitro and in vivo. The expression of CD25 and NF-κB activity do not differ between acute and chronic ATL cells.[12-15] These results suggest that anti-ATL activity of ritonavir correlates with suppression of NF-κB activity. It is also of interest to note that HTLV-I uses an aspartic protease analogous to HIV protease in its replication. To our knowledge, the activity of ritonavir against HTLV-I protease has not been assessed. Although Tax expression is very low or undetectable in ATL malignancy, a direct antiviral effect of ritonavir cannot be ruled out at this time.

In summary, using a large number of patient samples we have established a novel NOG ATL model that presents features similar to patients with ATL. These results also indicate that the HIV PI, ritonavir, showed antitumor and anti–NF-κB activity against primary ATL cells. Finally, our results strongly suggest that NF-κB serves as a potential molecular target to treat ATL, and that ritonavir might be used clinically as a single compound or in combination with the reducing dose of chemotherapeutic agents for treatment of patients with ATL.

Acknowledgments

We thank D. Kempf and T. Yamada of Abbott Laboratories, N. Yamamoto and S. Takeda of Molecular Virology, S. Ichinose of the Instrumental Analysis Research Center, S. Endo of the Animal Research Center, Tokyo Medical and Dental University, and P.J. Richard of Cardiff University for their advice and assistance with the experiments, and Y. Sato of the National Institute of Infectious Diseases for her excellent technical assistance. We thank J. Fujisawa for providing a luciferase reporter construct, κB-LUC, K. Matsumoto for providing the Tax expression plasmid, M. Maeda for providing ED-40 515(−), and the Fujisaki Cell Center, Hayashibara Biomedical Laboratories, for providing the MT-1, HUT-102, and C5/MJ cell lines.

References

1. Hinuma Y, Nagata K, Hanaoka M, et al. Adult T-cell leukemia: antigen in an ATL cell line and detection of antibodies to the antigen in human sera. Proc Natl Acad Sci U S A. 1981;78:6476-6480.
2. Poiesz BJ, Ruscetti FW, Gazdar AF, Bunn PA, Minna JD, Gallo RC. Detection and isolation of type C retrovirus particles from fresh and cultured lymphocytes of a patient with cutaneous T-cell lymphoma. Proc Natl Acad Sci U S A. 1980;77:7415-7419.
3. Yoshida M, Miyoshi I, Hinuma Y. Isolation and characterization of retrovirus from cell lines of human adult T-cell leukemia and its implication in the disease. Proc Natl Acad Sci U S A. 1982;79:2031-2035.
4. Takatsuki K, Uchiyama T, Sagawa K, Yodoi J. Adult T-cell leukemia in Japan. In: Seno S, Takaku F, Irino S, eds. Topics in Hematology. Amsterdam, The Netherlands: Excerpta Medica; 1977:73-77.
5. Uchiyama T, Yodoi J, Sagawa K, Takatsuki K, Uchino H. Adult T-cell leukemia: clinical and hematologic features of 16 cases. Blood. 1977;50:481-492.
6. Yamada Y, Tomonaga M, Fukuda H, et al. A new G-CSF-supported combination chemotherapy, LSG15, for adult T-cell leukaemia-lymphoma: Japan Clinical Oncology Group Study 9303. Br J Haematol. 2001;113:375-382.
7. Felber BK, Paskalis H, Kleinman-Ewing C, Wong-Staal F, Pavlakis GN. The pX protein of HTLV-I is a transcriptional activator of its long terminal repeats. Science. 1985;229:675-679.
8. Sodroski JG, Rosen CA, Haseltine WA. Trans-acting transcriptional activation of the long terminal repeat of human T lymphotropic viruses in infected cells. Science. 1984;225:381-385.
9. Maruyama M, Shibuya H, Harada H, et al. Evidence for aberrant activation of the interleukin-2 autocrine loop by HTLV-1-encoded p40x and T3/Ti complex triggering. Cell. 1987;48:343-350.
10. Ballard DW, Bohnlein E, Lowenthal JW, Wano Y, Franza BR, Greene WC. HTLV-I tax induces cellular proteins that activate the κB element in the IL-2 receptor α gene. Science. 1988;241:1652-1655.
11. Cross SL, Feinberg MB, Wolf JB, Holbrook NJ, Wong-Staal F, Leonard WJ Regulation of the human interleukin-2 receptor α chain promoter: activation of a nonfunctional promoter by the transactivator gene of HTLV-I. Cell. 1987;49:47-56.
12. Uchiyama T, Broder S, Waldmann TA. A monoclonal antibody (anti-Tac) reactive with activated and functionally mature human T cells, I: production of anti-Tac monoclonal antibody and distribution of Tac (+) cells. J Immunol. 1981;126:1393-1397.
13. Uchiyama T, Hori T, Tsudo M, et al. Interleukin-2 receptor (Tac antigen) expressed on adult T cell leukemia cells. J Clin Invest. 1985;76:446-453.
14. Waldmann TA, Greene WC, Sarin PS, et al. Functional and phenotypic comparison of human T cell leukemia/lymphoma virus positive adult T cell leukemia with human T cell leukemia/lymphoma virus negative Sezary leukemia, and their distinction using anti-Tac. Monoclonal antibody identifying the human receptor for T cell growth factor. J Clin Invest. 1984;73:1711-1718.
15. Mori N, Fujii M, Ikeda S, et al. Constitutive activation of NF-κB in primary adult T-cell leukemia cells. Blood. 1999;93:2360-2368.
16. Baldwin AS. The NF-κB and IκB proteins: new discoveries and insights. Annu Rev Immunol. 1999;14:649-681.
17. Watanabe M, Dewan MZ, Okamura T, et al. A novel NF-κB inhibitor DHMEQ selectively targets constitutive NF-κB activity and induces apoptosis of multiple myeloma cells in vitro and in vivo. Int J Cancer. 2005;114:32-38.
18. Adams J, Palombella VJ, Elliott PJ. Proteasome inhibition: a new strategy in cancer treatment. Invest New Drugs. 2000;18:109-121.
19. Teicher BA, Ara G, Herbst R, Palombella VJ, Adams J. The proteasome inhibitor PS-341 in cancer therapy. Clin Cancer Res. 1999;5:2638-2645.
20. Hideshima T, Chauhan D, Richardson P, et al. NF-κB as a therapeutic target in multiple myeloma. J Biol Chem. 2002;277:16639-16647.
21. Dewan MZ, Terashima K, Taruishi M, et al. Rapid tumor formation of human T-cell leukemia virus type 1-infected cell lines in novel NOD-SCID/γc^{null} mice: suppression by an inhibitor against NF-κB. J Virol. 2003;77:5286-5294.
22. Kitajima I, Shinohara T, Bilakovics J, Brown DA, Xu X, Nerenberg M. Ablation of transplanted HTLV-I Tax-transformed tumors in mice by antisense inhibition of NF-κB. Science. 1992;258:1792-1795.
23. Mori N, Yamada Y, Ikeda S, et al. Bay 11-7082 inhibits transcription factor NF-κB and induces apoptosis of HTLV-I–infected T-cell lines and primary adult T-cell leukemia cells. Blood. 2002;100:1828-1834.
24. Tan C, Waldmann TA. Proteasome inhibitor PS-341, a potential therapeutic agent for adult T-cell leukemia. Cancer Res. 2002;62:1083-1086.
25. Collier AC. Efficacy of combination antiretroviral therapy. Adv Exp Med Biol. 1996;394:355-372.
26. Collier AC, Coombs RW, Schoenfeld DA, Bassett R, Baruch A, Corey L. Combination therapy with zidovudine, didanosine and saquinavir. Antiviral Res. 1996;29:99.
27. Collier AC, Coombs RW, Schoenfeld DA, et al. Treatment of human immunodeficiency virus infection with saquinavir, zidovudine, and zalcitabine. AIDS Clinical Trials Group. N Engl J Med. 1996;334:1011-1017.
28. Markowitz M, Saag M, Powderly WG, et al. A preliminary study of ritonavir, an inhibitor of HIV-1 protease, to treat HIV-1 infection. N Engl J Med. 1995;333:1534-1539.
29. Kempf DJ, Marsh KC, Denissen JF, et al. ABT-538 is a potent inhibitor of human immunodeficiency virus protease and has high oral bioavailability in humans. Proc Natl Acad Sci U S A. 1995;92:2484-2488.
30. Andre P, Groettrup M, Klenerman P, et al. An inhibitor of HIV-1 protease modulates proteasome activity, antigen presentation, and T cell responses. Proc Natl Acad Sci U S A. 1998;95:13120-13124.
31. Liang JS, Distler O, Cooper DA, Jamil H, Deckelbaum RJ, Ginsberg HN, Sturley SL. HIV protease inhibitors protect apolipoprotein B from degradation by the proteasome: a potential mechanism for protease inhibitor-induced hyperlipidemia. Nat Med. 2001;7:1327-1331.
32. Schmidtke G, Holzhutter HG, Bogyo M, et al. How an inhibitor of the HIV-I protease modulates proteasome activity. J Biol Chem. 1999;274:35734-35740.
33. Gaedicke S, Firat-Geier E, Constantiniu O, et al. Antitumor effect of the human immunodeficiency virus protease inhibitor ritonavir: induction of tumor-cell apoptosis associated with perturbation of proteasomal proteolysis. Cancer Res. 2002;62:6901-6908.
34. Pati S, Pelser CB, Dufraine J, Bryant JL, Reitz MS Jr, Weichold FF. Antitumorigenic effects of HIV protease inhibitor ritonavir: inhibition of Kaposi sarcoma. Blood. 2002;99:3771-3779.
35. Sgadari C, Barillari G, Toschi E, et al. HIV protease inhibitors are potent anti-angiogenic molecules and promote regression of Kaposi sarcoma. Nat Med. 2002;8:225-232.
36. Miyoshi I, Kubonishi I, Yoshimoto S, et al. Type C virus particles in a cord T-cell line derived by cocultivating normal human cord leukocytes and

human leukaemic T cells. Nature. 1981;294:770-771.

37. Yamamoto N, Okada M, Koyanagi Y, Kannagi M, Hinuma Y. Transformation of human leukocytes by cocultivation with an adult T cell leukemia virus producer cell line. Science. 1982;217:737-739.
38. Popovic M, Sarin PS, Robert-Gurroff M, et al. Isolation and transmission of human retrovirus (human T-cell leukemia virus). Science. 1983;219:856-859.
39. Koeffler HP, Chen IS, Golde DW. Characterization of a novel HTLV-infected cell line. Blood. 1984;64:482-490.
40. Miyoshi I, Kubonishi I, Sumida M, et al. A novel T-cell line derived from adult T-cell leukemia. Gann. 1980;71:155-156.
41. Maeda M, Shimizu A, Ikuta K, et al. Origin of human T-lymphotrophic virus I-positive T cell lines in adult T cell leukemia. Analysis of T cell receptor gene rearrangement. J Exp Med. 1985;162:2169-2174.
42. Ishiyama M, Shiga M, Sasamoto K, Mizoguchi M, He P. A new sulfonated tetrazolium salt that produces a highly water-soluble formazan dye. Chem Pharm Bull. 1993;41:1118-1122.
43. Zhang C, Ao Z, Seth A, Schlossman SF. A mitochondrial membrane protein defined by a novel monoclonal antibody is preferentially detected in apoptotic cells. J Immunol. 1996;157:3980-3987.
44. Seth A, Zhang C, Letvin NL, Schlossman SF. Detection of apoptotic cells from peripheral blood of HIV-infected individuals using a novel monoclonal antibody. AIDS. 1997;11:1059-1061.
45. Matsumoto K, Shibata H, Fujisawa J, et al. Human T-cell leukemia virus type 1 Tax protein transforms rat fibroblasts via two distinct pathways. J Virol. 1997;71:4445-4451.
46. Dewan MZ, Watanabe M, Terashima K, et al. Prompt tumor formation and maintenance of constitutive NF-κB activity of multiple myeloma cells in NOD/SCID/γc^{null} mice. Cancer Sci. 2004;95:1-5.
47. Duyao MP, Kessler DJ, Spicer DB, et al. Transactivation of the c-myc promoter by human T cell leukemia virus type 1 tax is mediated by NFκB. J Biol Chem. 1992;267:16288-16291.
48. Huang Y, Ohtani K, Iwanaga R, Matsumura Y, Nakamura M. Direct trans-activation of the human cyclin D2 gene by the oncogene product Tax of human T-cell leukemia virus type I. Oncogene. 2001;20:1094-1102.
49. Mitsiades N, Mitsiades CS, Poulaki V, et al. Biologic sequelae of nuclear factor-κB blockade in multiple myeloma: therapeutic applications. Blood. 2002;99:4079-4086.
50. Mori N, Fujii M, Cheng G, et al. Human T-cell leukemia virus type I tax protein induces the expression of anti-apoptotic gene Bcl-x_L in human T-cells through nuclear factor-κB and c-AMP responsive element binding protein pathways. Virus Genes. 2001;22:279-287.
51. Nicot C, Mahieux R, Takemoto S, Franchini G. Bcl-X_L is up-regulated by HTLV-I and HTLV-II in vitro and in ex vivo ATLL samples. Blood. 2000;96:275-281.
52. Tamura K. Clinical classification of adult T-cell leukemia and its complications. Rinsho Byori. 1996;44:19-23.
53. Watanabe T. HTLV-1-associated diseases. Int J Hematol. 1997;66:257-278.
54. Imada K, Takaori-Kondo A, Sawada H, et al. Serial transplantation of adult T cell leukemia cells into severe combined immunodeficient mice. Jpn J Cancer Res. 1996;87:887-892.
55. Kondo A, Imada K, Hattori T, et al. A model of in vivo cell proliferation of adult T-cell leukemia. Blood. 1993;82:2501-2509.
56. Phillips KE, Herring B, Wilson LA, et al. IL-2Rα-directed monoclonal antibodies provide effective therapy in a murine model of adult T-cell leukemia by a mechanism other than blockade of IL-2/IL-2Rα interaction. Cancer Res. 2000;60:6977-6984.
57. Chu ZL, McKinsey TA, Liu L, Gentry JJ, Malim MH, Ballard DW. Suppression of tumor necrosis factor-induced cell death by inhibitor of apoptosis c-IAP2 is under NF-κB control. Proc Natl Acad Sci U S A. 1997;94:10057-10062.
58. Norvir, ritonavir product monograph. North Chicago, IL: Abbott Laboratories, 1997.
59. Gatti G, Di Biagio A, Casazza R, et al. The relationship between ritonavir plasma levels and side-effects: implications for therapeutic drug monitoring. AIDS. 1999;13:2083-2089.

ARTICLE

OBC

www.rsc.org/obc

Structure–activity relationship studies on CXCR4 antagonists having cyclic pentapeptide scaffolds†

Hirokazu Tamamura,*[a,b] Ai Esaka,[b] Teppei Ogawa,[b] Takanobu Araki,[b] Satoshi Ueda,[b] Zixuan Wang,[c] John O. Trent,[d] Hiroshi Tsutsumi,[a] Hiroyuki Masuno,[a] Hideki Nakashima,[e] Naoki Yamamoto,[f] Stephen C. Peiper,[c] Akira Otaka[b,g] and Nobutaka Fujii*[b]

[a] *Institute of Biomaterials and Bioengineering, Tokyo Medical and Dental University, Chiyoda-ku, Tokyo, 101-0062, Japan. E-mail: tamamura.mr@tmd.ac.jp; Fax: +81 3 5280 8039; Tel: +81 3 5280 8036*

[b] *Graduate School of Pharmaceutical Sciences, Kyoto University, Sakyo-ku, Kyoto, 606-8501, Japan. E-mail: nfujii@pharm.kyoto-u.ac.jp; Fax: +81 75 753 4570; Tel: +81 75 753 4551*

[c] *Medical College of Georgia, Augusta, GA, 30912, USA*

[d] *James Graham Brown Cancer Center, University of Louisville, Louisville, KY, 40202, USA*

[e] *St. Marianna University, School of Medicine, Miyamae-ku, Kawasaki, 216-8511, Japan*

[f] *AIDS Research Center, National Institute of Infectious Diseases, Shinjuku-ku, Tokyo, 162-8640, Japan*

[g] *Graduate School of Pharmaceutical Sciences, The University of Tokushima, Tokushima, 770-8505, Japan*

Received 19th September 2005, Accepted 26th October 2005
First published as an Advance Article on the web 15th November 2005

Structure–activity relationship studies on CXCR4 antagonists, which were previously found by using cyclic pentapeptide libraries, were performed to optimize side-chain functional groups, involving conformationally constrained analogues. In addition, a new lead of cyclic pentapeptides with the introduction of a novel pharmacophore was developed.

Introduction

Chemokine receptors belong to a superfamily of seven transmembrane G-protein coupled receptors (7TM-GPCRs). An axis of a chemokine receptor, CXCR4, and its endogenous ligand, stromal cell-derived factor-1 (SDF-1/CXCL12),[1] has multiple important functions in normal physiology involving the migration of progenitors during embryologic development of the cardiovascular, hemopoietic and central nervous systems. This axis has been also recognized to be involved in several pathological conditions, such as HIV infection,[2] cancer metastasis/progression[3] and rheumatoid arthritis (RA).[4] Initially, CXCR4 was identified as a co-receptor that is used in the entry of T cell line-tropic (X4-) HIV-1 into T cells.[2] Subsequently, several papers reported that malignant cells from different types of cancer express CXCR4,[5] and that CXCL12 is highly expressed in the major metastatic destinations of the corresponding cancer,[3] suggesting that the interaction between CXCR4 and CXCL12 might determine the metastatic destination of cancer cells and cause organ preferential metastasis. Furthermore, Nanki *et al.* reported that CXCL12, which is highly expressed in the synovium of RA patients, stimulates migration of the memory T cells, which highly express CXCR4, thereby inhibits T cell apoptosis and leads to T cell accumulation in the RA synovium.[4a] Thus, CXCR4 is thought to be a great therapeutic target. A 14-mer peptide T140 and its analogues were previously found to be specific CXCR4 antagonists that were characterized as HIV-entry inhibitors,[6] anti-cancer-metastatic agents[3c] and anti-RA agents.[4b] The utilization of cyclic pentapeptide libraries involving the critical residues of T140, which were previously identified to be Arg^2, L-3-(2-naphthyl)alanine $(Nal)^3$, Tyr^5 and Arg^{14},[7] led to the finding of a cyclic pentapeptide FC131 [*cyclo*(-Arg^1-Arg^2-Nal^3-Gly^4-D-Tyr^5-)], which has strong CXCR4 antagonistic activity, comparable to that of T140 (Fig. 1).[8] Several FC131 analogues constrained or modified in Arg^1 were synthesized to find useful leads.[9] In this paper, we describe structure–activity relationship (SAR) studies on FC131 based on several synthetic analogues, which involve substitution for Arg^2, Nal^3 and D-Tyr^5. In addition, we attempt to incorporate a new pharmacophore such as a 4-fluorophenyl moiety, which was previously identified by the *N*-terminal modification of T140 analogs,[10] into cyclic pentapeptides.

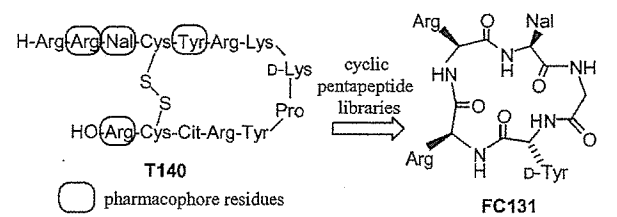

Fig. 1 Development of a low molecular weight CXCR4 antagonist FC131 based on cyclic pentapeptide libraries. Cit = L-citrulline.

Chemistry

Each peptide was synthesized in a general manner.[8] In the synthesis of compounds **6**, **7**, **9** and **10**, after cyclization and deprotection, *N*-guanylation of the resulting free side-chain amino group was performed with 1*H*-pyrazole-1-carboxamidine hydrochloride and DIPEA.[9]

Biological results and discussion

Several FC131 analogues, which have substitution for Arg^2, Nal^3 and D-Tyr^5, were prepared and assessed for CXCR4-binding activity based on inhibitory activity against CXCL12 binding to CXCR4.[11] First, analogues modified in the peripheral region of

† Electronic supplementary information (ESI) available: Characterization data (MS) of novel synthetic compounds. See DOI: 10.1039/b513145f

DOI: 10.1039/b513145f

Table 1 Inhibitory activity of cyclic pentapeptides involving substitution for Arg^2 in FC131 against CXCL12 binding to CXCR4

Compd	*cyclo*(-Arg^1-X-Nal^3-Gly^4-D-Tyr^5-) X	IC_{50}/μM[a]
1 (FC131)	Arg	0.0079
2	Ala	>1
3	Dab	0.44
4	Orn	0.69
5	Lys	>1
6	g-Dab	1.1
7	g-Lys	0.033
8	Glu	>1
9	*trans*-4-Guanidino-Pro	>1
10	*cis*-4-Guanidino-Pro	>1

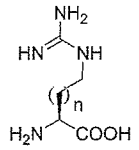

n = 1 γ-*N*-amidino-Dab (g-Dab)
n = 3 ε-*N*-amidino-Lys (g-Lys)

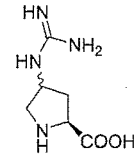

trans/*cis*-4-guanidino-Pro

[a] IC_{50} values are based on the inhibition of [^{125}I]-CXCL12 binding to CXCR4 transfectants of CHO cells. All data are mean values for at least three independent experiments.

Arg^2 were assayed (Table 1). Ala-substitution for Arg^2 in FC131 completely diminished the activity of the parent compound, whereas Ala-substitution for Arg^1 did not cause a severe decrease in potency,[9] suggesting that the side-chain of Arg^2 is very important for strong activity. Thus, optimization of the side-chain of Arg^2 was attempted by the synthesis of several analogues, where Arg^2 was replaced by Arg/Lys mimetics having various lengths of alkyl chains. L-2,4-Diaminobutyric acid (Dab)/L-ornithine (Orn)-substituted analogues, **3** and **4**, showed moderate CXCR4-binding activity, which is two orders of magnitude less potent than that of FC131, while a Lys-substituted analogue **5** did not show any significant activity until 1 μM. An ε-*N*-amidino-Lys (g-Lys)-substituted analogue, **7**, which has the side-chain with a one-carbon elongation compared to Arg^2, showed significant CXCR4-binding activity, which is 4-fold weaker than FC131. A γ-*N*-amidino-Dab (g-Dab)-substituted analogue, **6**, which has the side-chain with a one-carbon reduction compared to Arg^2, showed very low activity. It suggests that Arg is the most suitable at position 2 among the Arg/Lys mimetics used in this study. A Glu-substituted analogue, **8**, did not show any significant activity until 1 μM, suggesting that a basic functional group, such as an amino or guanidino group, in the side-chain of the amino acid at position 2 is indispensable for binding to CXCR4. In our previous study, analogues, in which a conformationally constrained Arg mimetic, *trans*- or *cis*-4-guanidino-Pro, was incorporated at position 1, showed higher CXCR4-binding activity than a g-Dab-substituted analogue, having the same length of the linear-type side chain of the amino acid at position 1.[9] Thus, in this study, analogues, in which *trans*- or *cis*-4-guanidino-Pro was incorporated at position 2, were prepared and assessed for CXCR4-binding activity. However, the conformationally constrained analogues, **9** and **10**, did not show any significant activity until 1 μM. This proved that fixing the backbone and the side-chain of Arg^2 is not suitable.

Second, analogues modified in the peripheral region of Nal^3 were assayed (Table 2). Ala-substitution for Nal^3 in FC131 completely diminished the activity of the parent compound. Since the side-chain of Nal^3 is indispensable for strong activity, optimization of the side-chain of Nal^3 was attempted by the synthesis of several analogues, where Nal^3 was replaced by Trp mimetics. A Trp-substituted analogue, **12**, showed strong CXCR4-binding activity, which is slightly less potent than

Table 2 Inhibitory activity of cyclic pentapeptides involving substitution for Nal^3 in FC131 against CXCL12 binding to CXCR4

Compd	*cyclo*(-Arg^1-Arg^2-X-Gly^4-D-Tyr^5-) X	IC_{50}/μM
1 (FC131)	Nal	0.0079
11	Ala	>1
12	Trp	0.013
13	Tpi	>1
14	Bth	0.018
15	D-Bth	0.26

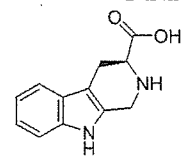

(3*S*)-2,3,4,9-tetrahydro-1*H*-β-carboline-3-carboxylic acid (Tpi)

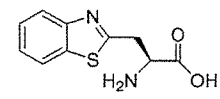

(2*S*)-2-amino-3-benzothiazol-2-yl-propionic acid (Bth)

that of FC131. This is compatible with our previous result: T140 is more potent than T134 [Trp^3-T140].[6] A (3*S*)-2,3,4,9-tetrahydro-1*H*-β-carboline-3-carboxylic acid (Tpi)-substituted analogue, **13**, which is conformationally constrained in the backbone and the side-chain of the amino acid at position 3, did not show any significant activity until 1 μM, suggesting that fixing the backbone and the side-chain of Trp (or Nal^3) is not suitable. A (2*S*)-2-amino-3-benzothiazol-2-yl-propionic acid (Bth)-substituted analogue, **14**, showed strong CXCR4-binding activity, which is almost the same as that of the Trp-substituted analogue, **12**. D-Bth-substituted analogue, **15**, is 14-fold less potent than **14**. This is also compatible with our previous result: D-Nal^3-FC131 is 20-fold less potent than FC131.[8] Taken together, Nal is more suitable at position 3 than any other Trp-mimetics.

Third, analogues modified in the peripheral region of D-Tyr^5 were assayed (Table 3). D-Ala-substitution for D-Tyr^5 in FC131 also diminished the activity of the parent compound. Optimization of the side-chain of D-Tyr^5 was attempted by the synthesis of several analogues, where D-Tyr^5 was replaced by D-Tyr/Phe mimetics. A D-Phe(4-NH_2)-substituted analogue, **17**, and a D-Phe(4-OMe)-substituted analogue, **18**, which have electron-donating substituents on the aromatic ring of the amino acid at position 5, showed remarkably less potent CXCR4-binding activity than FC131, which also has an electron-donating substituent on the aromatic ring. The analogues, **17** and **18**, were weaker than a D-Phe-substituted analogue,

Table 3 Inhibitory activity of cyclic pentapeptides involving substitution for D-Tyr^5 in FC131 against CXCL12 binding to CXCR4

Compd	*cyclo*(-Arg^1-Arg^2-Nal^3-Gly^4-X-) X	IC_{50}/μM
1 (FC131)	D-Tyr	0.0079
16	D-Ala	>1
17	4-Amino-D-phenylalanine [D-Phe(4-NH_2)]	0.10
18	4-Methoxy-D-phenylalanine [D-Phe(4-OMe)]	0.51
19	D-His	0.15
20	D-Phe	0.051
21	4-Fluoro-D-phenylalanine [D-Phe(4-F)]	0.22
22	D-Tic(7-OH)	0.16

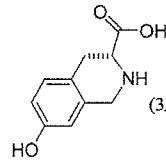

(3*R*)-7-Hydroxy-1,2,3,4-tetrahydro-isoquinoline-3-carboxylic acid [D-Tic(7-OH)]

Table 4 Inhibitory activity of cyclic pentapeptides involving the incorporation of Phe(4-F)^1 into FC131 against CXCL12 binding to CXCR4

Compd	Sequence	$IC_{50}/\mu M$
1 (FC131)	*cyclo*(-Arg^1-Arg^2-Nal^3-Gly^4-D-Tyr^5-)	0.0079
23	*cyclo*(-Phe(4-F)^1-Arg^2-Nal^3-Gly^4-D-Tyr^5-)	0.057
24	*cyclo*(-Phe(4-F)^1-Arg^2-Nal^3-Gly^4-Arg^5-)	0.62
25	*cyclo*(-D-Phe(4-F)^1-Arg^2-Nal^3-Gly^4-Arg^5-)	0.035
26	*cyclo*(-Phe(4-F)^1-Arg^2-Nal^3-Gly^4-D-Arg^5-)	0.088
27	*cyclo*(-D-Phe(4-F)^1-Arg^2-Nal^3-Gly^4-D-Arg^5-)	0.094
28	*cyclo*(-D-Tyr^1-Arg^2-Nal^3-Gly^4-Arg^5-)	0.30

20. Thus, an electron-donating substituent on the aromatic ring of the amino acid at position 5 is not always suitable for strong CXCR4-binding activity. On the other hand, a D-Phe(4-F)-substituted analogue, **21**, which has an electron-withdrawing substituent on the aromatic ring, was also less potent than FC131 or the D-Phe-substituted analogue, **20**. A D-His-substituted analogue, **19**, which has a basic/aromatic amino acid at position 5, did not show stronger activity than **20**. A (3*R*)-7-hydroxy-1,2,3,4-tetrahydro-isoquinoline-3-carboxylic acid [D-Tic(7-OH)]-substituted analogue, **22**, which is conformationally constrained in the backbone and the side-chain of the amino acid at position 5, showed remarkably less potent CXCR4-binding activity than FC131, suggesting that fixing the backbone and the side-chain of D-Tyr^5 is also not suitable. Taken together, D-Tyr is the most suitable at position 5 among the tested amino acids without any relation to the electron-withdrawing or -donating effect of the substituent on the aromatic ring.

Recently, a novel pharmacophore of T140-related CXCR4 antagonists, such as a 4-fluorophenyl moiety, was found in addition to the original pharmacophores of T140, Arg (x 2), Nal and Tyr.[10] Fourth, since the phenol group of D-Tyr^5 could not be replaced by the 4-fluorophenyl group with maintenance of high activity, as seen in the D-Phe(4-F)-substituted analogue, **21**, we attempted to incorporate the 4-fluorophenyl group into the amino acid at position 1. [Phe(4-F)^1]-FC131, **23**, showed significant CXCR4-binding activity, which is less potent than that of FC131. Since another Arg residue is thought to be indispensable for high activity and an aromatic residue [L/D-Phe(4-F)] is incorporated into position 1, we tried to replace D-Tyr^5 by L/D-Arg^5. Four analogues, **24–27**, [L/D-Phe(4-F)^1, L/D-Arg^5]-FC131, were prepared and assayed (Table 4). Among these compounds [D-Phe(4-F)^1, Arg^5]-FC131, **25**, showed the most potent activity, which is 10-fold more potent than that of [D-Tyr^1, Arg^5]-FC131, **28**. Thus, it is thought that [D-Phe(4-F)^1, Arg^5]-FC131, **25**, is useful as a novel lead involving the pharmacophores different from FC131, although **25** is 4-fold less potent than FC131.

Conclusion

In summary, SAR studies on cyclic pentapeptides having CXCR4-antagonistic activity, such as FC131, were performed. Several analogues were synthesized to optimize side-chain functional groups, involving constrained analogues that conformationally fix the backbone and the side-chains. Taken together, Arg, Nal and D-Tyr are the most suitable at position 2, 3 and 5, respectively, than any other corresponding amino acid mimetics that were tested in the present study. Furthermore, a novel lead compound, which contains a 4-fluorophenyl group as the new pharmacophore, was found.

Acknowledgements

This work was supported in part by a 21st Century COE Program "Knowledge Information Infrastructure for Genome Science", a Grant-in-Aid for Scientific Research from the Ministry of Education, Culture, Sports, Science and Technology, Japan, the Japan Health Science Foundation and Philip Morris USA Inc. and Philip Morris International. S. U. is grateful for a Research Fellowship from the Japan Society for the Promotion of Science for Young Scientists.

References

1 (*a*) T. Nagasawa, H. Kikutani and T. Kishimoto, *Proc. Natl. Acad. Sci. U. S. A.*, 1994, **91**, 2305; (*b*) C. C. Bleul, M. Farzan, H. Choe, C. Parolin, I. Clark-Lewis, J. Sodroski and T. A. Springer, *Nature*, 1996, **382**, 829; (*c*) E. Oberlin, A. Amara, F. Bachelerie, C. Bessia, J.-L. Virelizier, F. Arenzana-Seisdedos, O. Schwartz, J.-M. Heard, I. Clark-Lewis, D. F. Legler, M. Loetscher, M. Baggiolini and B. Moser, *Nature*, 1996, **382**, 833; (*d*) K. Tashiro, H. Tada, R. Heilker, M. Shirozu, T. Nakano and T. Honjo, *Science*, 1993, **261**, 600.

2 Y. Feng, C. C. Broder, P. E. Kennedy and E. A. Berger, *Science*, 1996, **272**, 872.

3 (*a*) T. Koshiba, R. Hosotani, Y. Miyamoto, J. Ida, S. Tsuji, S. Nakajima, M. Kawaguchi, H. Kobayashi, R. Doi, T. Hori, N. Fujii and M. Imamura, *Clin. Cancer Res.*, 2000, **6**, 3530; (*b*) A. Müller, B. Homey, H. Soto, N. Ge, D. Catron, M. E. Buchanan, T. McClanahan, E. Murphy, W. Yuan, S. N. Wagner, J. L. Barrera, A. Mohar, E. Verastegui and A. Zlotnik, *Nature*, 2001, **410**, 50; (*c*) H. Tamamura, A. Hori, N. Kanzaki, K. Hiramatsu, M. Mizumoto, H. Nakashima, N. Yamamoto, A. Otaka and N. Fujii, *FEBS Lett.*, 2003, **550**, 79; (*d*) N. Tsukada, J. A. Burger, N. J. Zvaifler and T. J. Kipps, *Blood*, 2002, **99**, 1030; (*e*) J. Juarez, K. F. Bradstock, D. J. Gottlieb and L. J. Bendall, *Leukemia*, 2003, **17**, 1294.

4 (*a*) T. Nanki, K. Hayashida, H. S. EI-Gabalawy, S. Suson, K. Shi, H. J. Girschick, S. Yavuz and P. E. Lipsky, *J. Immunol.*, 2000, **165**, 6590; (*b*) H. Tamamura, M. Fujisawa, K. Hiramatsu, M. Mizumoto, H. Nakashima, N. Yamamoto, A. Otaka and N. Fujii, *FEBS Lett.*, 2004, **569**, 99.

5 F. Balkwill, *Semin. Cancer Biol.*, 2004, **14**, 171.

6 H. Tamamura, Y. Xu, T. Hattori, X. Zhang, R. Arakaki, K. Kanbara, A. Omagari, A. Otaka, T. Ibuka, N. Yamamoto, H. Nakashima and N. Fujii, *Biochem. Biophys. Res. Commun.*, 1998, **253**, 877.

7 H. Tamamura, A. Omagari, S. Oishi, T. Kanamoto, N. Yamamoto, S. C. Peiper, H. Nakashima, A. Otaka and N. Fujii, *Bioorg. Med. Chem. Lett.*, 2000, **10**, 2633.

8 N. Fujii, S. Oishi, K. Hiramatsu, T. Araki, S. Ueda, H. Tamamura, A. Otaka, S. Kusano, S. Terakubo, H. Nakashima, J. A. Broach, J. O. Trent, Z. Wang and S. C. Peiper, *Angew. Chem., Int. Ed.*, 2003, **42**, 3251.

9 H. Tamamura, T. Araki, S. Ueda, Z. Wang, S. Oishi, A. Esaka, J. O. Trent, H. Nakashima, N. Yamamoto, S. C. Peiper, A. Otaka and N. Fujii, *J. Med. Chem.*, 2005, **48**, 3280.

10 H. Tamamura, K. Hiramatsu, M. Mizumoto, S. Ueda, S. Kusano, S. Terakubo, M. Akamatsu, N. Yamamoto, J. O. Trent, Z. Wang, S. C. Peiper, H. Nakashima, A. Otaka and N. Fujii, *Org. Biomol. Chem.*, 2003, **1**, 3663.

11 H. Tamamura, K. Hiramatsu, S. Ueda, Z. Wang, S. Kusano, S. Terakubo, J. O. Trent, S. C. Peiper, N. Yamamoto, H. Nakashima, A. Otaka and N. Fujii, *J. Med. Chem.*, 2005, **48**, 380.

Kisspeptin-10-Induced Signaling of GPR54 Negatively Regulates Chemotactic Responses Mediated by CXCR4: a Potential Mechanism for the Metastasis Suppressor Activity of Kisspeptins

Jean-Marc Navenot,[1] Zixuan Wang,[1] Michael Chopin,[1] Nobutaka Fujii,[2] and Stephen C. Peiper[1]

[1]Department of Pathology and Immunotherapy Center, Medical College of Georgia, Augusta, Georgia and [2]Graduate School of Pharmaceutical Sciences, Kyoto University, Sakyo-ku, Kyoto, Japan

Abstract

The product of the *KiSS-1* gene is absent or expressed at low level in metastatic melanoma and breast cancer compared with their nonmetastatic counterparts. A polypeptide derived from the KiSS-1 product, designated kisspeptin-10 (Kp-10), activates a receptor coupled to Gαq subunits (GPR54 or KiSS-1R). To study the mechanism by which Kp-10 antagonizes metastatic spread, the effect on CXCR4-mediated signaling, which has been shown to direct organ-specific migration of tumor cells, was determined. Kp-10 blocked chemotaxis of tumor cells expressing CXCR4 in response to low and high concentrations of SDF-1/CXCL12 and inhibited mobilization of calcium ions induced by this ligand. Pretreatment with Kp-10 did not induce down-modulation of cell surface CXCR4 expression, reduce affinity for SDF-1/CXCL12, or alter Gαi subunit activation stimulated by this ligand. Although Kp-10 stimulated prolonged phosphorylation of extracellular signal-regulated kinase 1/2, it inhibited the phosphorylation of Akt induced by SDF-1. The ability of Kp-10 to inhibit signaling and chemotaxis induced by SDF-1 indicates that activation of GPR54 signaling may negatively regulate the role of CXCR4 in programming tumor metastasis. (Cancer Res 2005; 65(22): 10450-6)

Introduction

The capacity for metastatic spread is a critical aspect of tumor cell biology that has a profound effect on clinical behavior. There is significant evidence that the metastatic phenotype is a composite effect of multiple mechanisms, including breach of normal architectural boundaries, angiogenesis, directed migration, and target site modification. Expression microarray analysis of high bone metastatic variants biologically selected from a nonmetastatic cell line identified *CXCR4* among a cadre of genes that confer the metastatic phenotype (1).

CXCR4, the receptor for the CXC chemokine stromal cell–derived factor 1 (SDF-1/CXCL12), is a G-protein-coupled receptor (GPCR) expressed by a wide spectrum of cells and its physiologic importance in hematopoiesis, development of the vasculature and of the central nervous system has been emphasized by the lethal phenotype of its knockout in mice. Among the candidate genes that were implicated in the metastatic phenotype, expression of CXCR4 alone was found to significantly increase the metastatic behavior, and bone metastasis was further increased by the coordinated expression of other prometastatic genes (1). Common target organs for the metastatic spread of breast cancer secrete SDF-1/CXCL12, including lung, lymph node, liver, and bone marrow. Blockade of this receptor with a monoclonal antibody has been shown to inhibit spread of human breast cancer cells to lungs and regional lymph nodes in a mouse xenograft model (2). Although CXCR4 has been implicated in the pathogenesis of metastatic spread of multiple malignant tumors, the regulation of this mechanism has not yet been elucidated (3). It is unclear whether expression of CXCR4 is sufficient to program migration of tumor cells to target organs that secrete SDF-1/CXCL12, or the sensitivity of this receptor to the chemotactic gradient of ligand may be positively and/or negatively regulated by independent factors.

Genes having a metastasis suppressor function are candidates for the negative regulation of prometastatic mechanisms (4). The *KiSS-1* gene was originally identified by its altered expression in metastatic melanoma but not in localized tumors (5). Programming of KiSS-1 expression in human breast carcinoma cell lines decreased metastatic spread in mouse xenograft models (6). The KiSS-1 protein (also known as metastin or kisspeptin) contains 145 residues and multiple shorter products resulting from naturally occurring proteolytic cleavage have been identified. Metastin (45-54) [also known as metastin (112-121) or KiSS-1 (112-121), kisspeptin-10 (Kp-10)] is a 10-residue peptide derived from the product of the KiSS-1 (7–11). Kisspeptins bind to the same GPCR (KiSS1-R: hOT7T175, AXOR12, and GPR54; refs. 7–9). Qualitatively, all the different forms of the polypeptide (natural or synthetic) have a similar activity but different affinities for their receptor, the decapeptide being the most active. Exposure of cancer cell lines (melanoma, pancreatic carcinoma, or Chinese hamster ovary, CHO) with endogenous or programmed expression of GPR54 to metastin decreased expression of metalloproteinase 9, motility, and proliferation *in vitro* and prevented metastasis *in vivo* (6–8, 12, 13). Because metastin decreased the motility and migration of cell lines exposed to fetal bovine serum (FBS), it was hypothesized that the antimetastatic action of this ligand may involve negative regulation of prometastatic mechanisms, including directed chemoattraction to target organs. In this study, the effect of Kp-10 on the function of CXCR4, including chemotaxis and intracellular signaling, was determined in CHO and HeLa cell transfectants.

Materials and Methods

Materials. The COOH-terminally amidated decapeptide Kp-10 (YNWNSFGLRF-NH_2) was synthesized at the University of Kyoto, Japan and was used in all the experiments. CHO and HeLa were selected because of their total absence of response to Kp-10 as assessed by calcium mobilization and activation of extracellular signal-regulated kinase 1/2 (ERK1/2)/mitogen-activated protein kinase (MAPK). CXCR4 is endogenous

Note: Supplementary data for this article are available at Cancer Research Online (http://cancerres.aacrjournals.org/).

Requests for reprints: Jean-Marc Navenot, Department of Pathology, Medical College of Georgia, BF212, 1120 15th Street, Augusta, GA 30912. Phone: 706-721-1409; Fax: 706-721-2358; E-mail: jnavenot@mcg.edu.

doi:10.1158/0008-5472.CAN-05-1757

in HeLa and expressed by transfection in CHO. Human GPR54 was subcloned in pcDNA3.1 (Invitrogen, Carlsbad, CA) with a Myc-tag at the NH_2 terminus and transfected in both cell lines. Transfectants were selected by magnetic sorting (Miltenyi Biotec, Auburn, CA).

Chemotaxis assay. Cells were resuspended in MEM-α/0.5% bovine serum albumin (BSA) at a density of 2×10^6/mL for CHO or 5×10^5 for HeLa, and 100 μL were added to the top chamber of 24-well transwell apparatus (6.5-mm diameter, 8.0-μm pore size; Corning, New York, NY) coated with collagen (human, type IV, Sigma, St Louis, MO). SDF-1 (Leinco Technologies, St Louis, MO) was added to the lower chamber, and Kp-10 was added either to the bottom chamber or both to the bottom and to the cells in the top chamber. The plates were incubated for 4 hours at 37°C. Cells were fixed with 20% ethanol/0.5% crystal violet, and the cells at the top of the membrane were wiped off. The cells on the bottom face of the membrane were stained with 4′,6-diamidino-2-phenylindole and counted with a fluorescence microscope. Alternatively, the cells migrating in the bottom chamber were resuspended in the medium and counted for 1 minute by flow cytometry (LSRII, Becton Dickinson, San Jose, CA) after appropriate gating.

Calcium mobilization. CHO cells were loaded with 2 μg/mL Fura-2 acetoxymethyl ester (Molecular Probes, Eugene, OR). Agonist-dependent increases in cytoplasmic calcium were determined as described (14). Calcium mobilization was also studied by flow cytometry. The cells were then prepared in a similar way except that Indo-1 (Molecular Probes) was used instead of Fura-2. The cells were analyzed on a LSRII flow cytometer equipped with a solid-state UV laser (Xcyte, Lightwave Electronics, Mountain View, CA). The fluorescence of Indo-1 was split by a 450-nm LP dichroic mirror and measured by two separate detectors after passage through a 530/30 band pass filter (calcium-free form) and a 405/20 band pass filter (calcium-bound form). Acquisition and analysis of the ratio of fluorescence over time was done with the Diva software (Becton Dickinson). About 300 cells per second were analyzed over the entire experiments.

Flow cytometry. Internalization of CXCR4 was measured by indirect immunofluorescence and flow cytometry. Cells were detached with citrate buffer, resuspended in MEM-α/0.5% BSA at 1×10^7 cells/mL. The cells (100 μL) were then exposed to 100 nmol/L of SDF-1 or 100 nmol/L of Kp-10 for 30 minutes at 37°C (or medium alone for the positive control). After an acid wash (pH 3) to elute the ligand from the receptor, cells were incubated with a saturating concentration of a monoclonal antibody to CXCR4 (A145, 10 μg/mL; ref. 15) followed by a phycoerythrin-labeled antibody to mouse IgG (Jackson ImmunoResearch Laboratories, West Grove, PA).

Ligand binding and displacement. Membrane preparations of CHO cells stably expressing the GPR54 were incubated with 0.1 nmol/L [^{125}I] metastin (45-54) (Amersham Biosciences, Piscataway, NJ) in the presence of incremental concentrations of Kp-10 as described previously (8). The affinity was calculated using Prism (GraphPad Software, San Diego, CA) and is expressed as the EC_{50} ± SD based on duplicate samples of each concentration.

γ[^{35}S]GTP binding assay. The γ[^{35}S]GTP binding assay was carried out as described previously (14). The effect of Kp-10 on the capacity of CXCR4 to activate G-proteins was measured either by incubating the membrane fraction with Kp-10 immediately before adding SDF-1 or following preincubation of the cells with Kp-10 for 5 minutes at 37°C to allow cross-desensitization before preparation of the membranes.

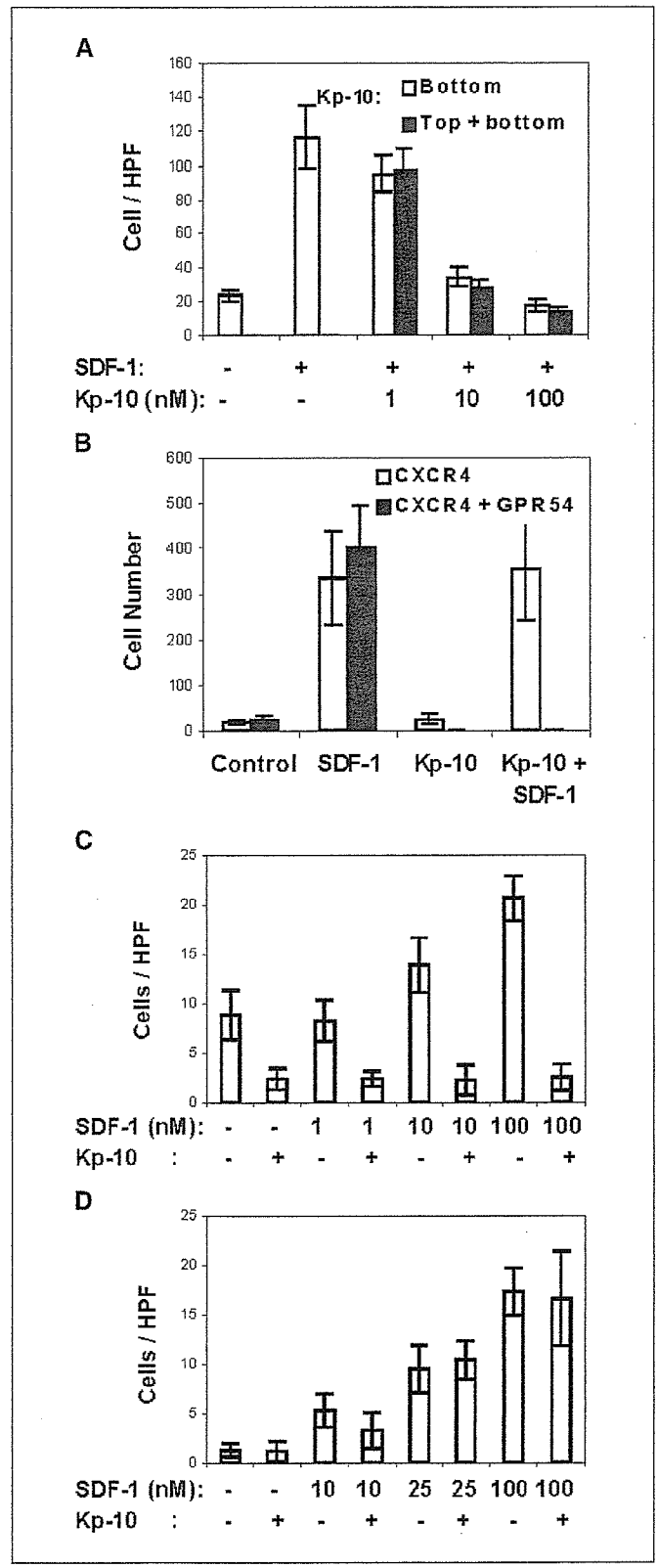

Figure 1. Kp-10 inhibits chemotaxis mediated by SDF-1 in CHO and HeLa cells expressing CXCR4 and the GPR54. *A*, Kp-10 inhibits chemotaxis toward 50 nmol/L of SDF-1 in a dose-dependent manner. The reduction of the number of migrating CHO cells depends on the concentration of Kp-10 ($P < 0.05$ at 1 nmol/L, $P < 0.001$ at 10 and 100 nmol/L), and the effect is independent of location in the top or the bottom chamber. Results are based on the number of cells counted in 8 high power fields (*HPF*, ×40) for each condition. *B*, the inhibitory effect of Kp-10 on CXCR4 requires the presence of GPR54 in CHO cells. Parallel experiments were done in triplicate in CXCR4 transfectants or CXCR4/GPR54 double transfectants. The cells in the bottom chamber of the transwell were counted for 1 minutes by flow cytometry. Almost no cells could be counted when GPR54 transfectants were exposed to Kp-10. *C*, inhibition of chemotaxis toward increasing doses of SDF-1 as well as chemokinesis is also observed in HeLa cells transfected with GPR54. Results are based on the number of cells counted in 8 high power fields and are representative of three independent experiments. *D*, Kp-10 does not inhibit chemotaxis or chemokinesis of HeLa cells that do not express the GPR54.

Western blot. CHO cells were seeded in 60-mm dishes (5×10^5), grown for 24 hours in MEM-α /10% FBS, and starved overnight in DMEM/0.5% BSA. Stimulation of the cells with 100 nmol/L of SDF-1 or Kp-10 or both was done at 37°C. The cells were then washed with ice-cold PBS and resuspended in lysis buffer (50 mmol/L Tris, 10 mmol/L EDTA, 150 mmol/L NaCl, 1% Triton X-100, 0.1% SDS, protease, and phosphatase inhibitors) for 1 hour. After centrifugation (15 minutes at 13,000 rpm), the soluble fraction was diluted in SDS sample buffer. SDS-PAGE and transfer to polyvinylidene difluoride were done according to standard protocols. Antibodies to p44/42 MAPK (ERK1/2), phospho-p44/42, Akt, phospho-Akt Ser^{473}, and phospho-Akt Thr^{308} (Cell Signaling Technology, Beverly, MA) were detected using horseradish peroxidase–labeled secondary antibodies (Jackson ImmunoResearch Laboratories) and Enhanced Chemiluminescence-Plus (Amersham Biosciences).

Statistics. When relevant, quantitative data were analyzed using the Student's *t* test.

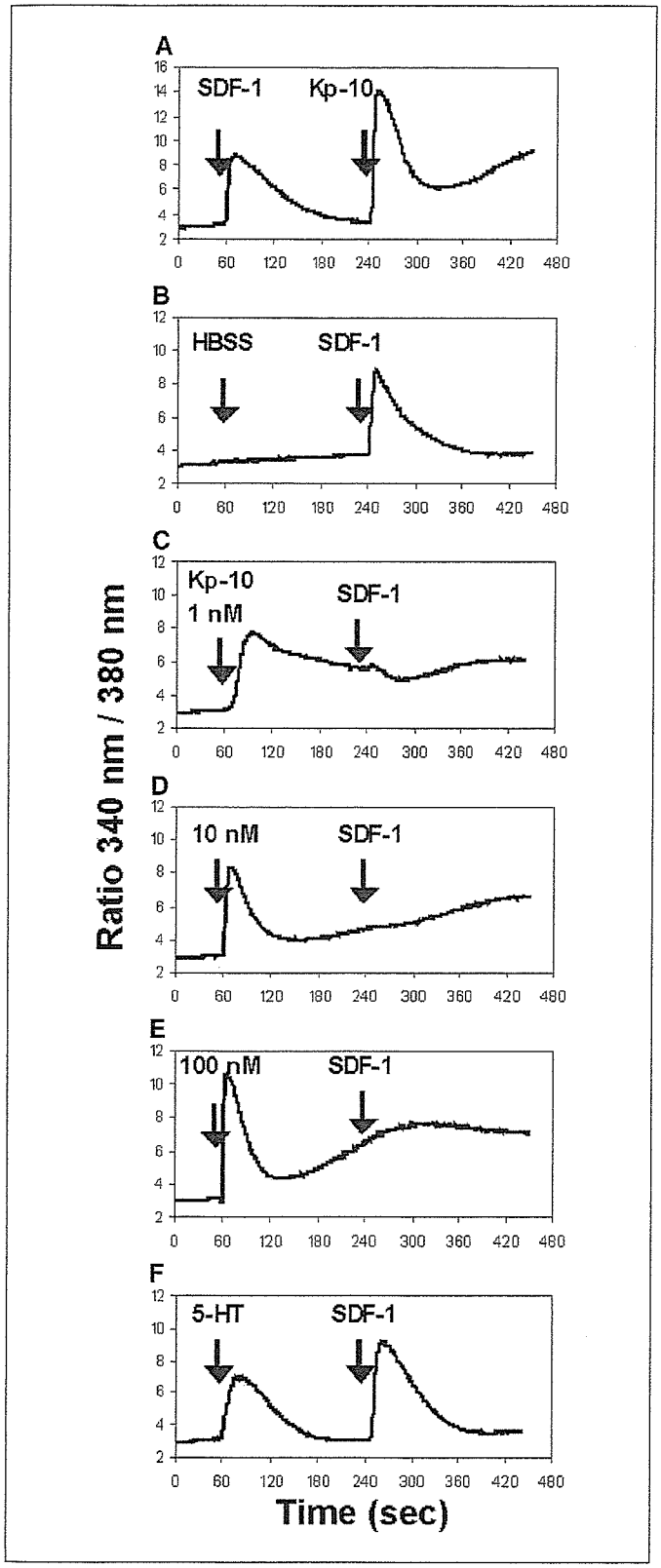

Results

KiSS-1 inhibits the chemotactic response to SDF-1. The findings related to the relative roles of CXCR4 and Kp-10 in cancer cell metastasis suggest that signaling induced by KiSS-1 may antagonize the effects of SDF-1, thereby suppressing the metastatic spread of breast cancer. The ability of Kp-10 to inhibit the directed migration induced by SDF-1 was tested in CHO transfectants expressing GPR54 and CXCR4. As shown in Fig. 1*A*, exposure of target cells to a gradient of Kp-10 parallel to a chemotactic gradient of SDF-1 inhibited chemotaxis induced by 50 nmol/L SDF-1 in a dose-dependent fashion. A similar suppression of chemotaxis induced by SDF-1 was noted when Kp-10 was placed in the upper chamber of the transwell and mixed with the cells immediately prior the initiation of chemotaxis (Fig. 1*A*). The presence of high concentration of Kp-10 (100 nmol/L) had no effect on SDF-1-induced chemotaxis of cells expressing CXCR4 but not GPR54 (Fig. 1*B*). Parallel experiments were done with HeLa cells, which have endogenous CXCR4 expression and were transfected with GPR54. As shown in Fig. 1*C*, exposure of HeLa-GPR54 transfectants to 100 nmol/L Kp-10 completely inhibited chemotaxis stimulated by SDF-1 at concentrations of 10 and 100 nmol/L. The magnitude of transmigration of cells exposed to Kp-10 was less than basal levels, consistent with the previous finding that kisspeptins decrease basal cytokinesis (8). Like in the case of CHO cells, no effect of Kp-10 on the chemotaxis induced by SDF-1 and CXCR4 was observed in HeLa cells that did not express the GPR54 (Fig. 1*D*). The transient nature of the suppressive effect on chemotaxis induced by SDF-1 was evident from the significant decrease in inhibition detected when chemotaxis to SDF-1 was initiated 4 hours following addition of Kp-10 (Supplementary Data 1).

Unilateral desensitization of CXCR4 signaling by GPR54 activation. The effect of GPR54 activation on CXCR4 signaling induced by SDF-1 was determined to elucidate potential mechanisms responsible for the suppression of chemotaxis stimulated by the latter ligand. Both Gi-coupled CXCR4 (and other chemotactic GPCRs) and Gq-coupled GPR54 can mobilize intracellular calcium by activating phospholipase C-β, either directly through the α subunit of Gq (GPR54) or through the Gβγ heterodimer (CXCR4). Crosstalk between GPCR can occur

Figure 2. Kp-10 inhibits the cytosolic calcium signaling response induced by the stimulation of CXCR4 by SDF-1 in CHO cells. Transfectants of CHO cells expressing CXCR4 and GPR54 were stimulated sequentially by SDF-1 or Kp-10. The addition of the first and the second ligand (*arrow*) are 3 minutes apart. *A*, cells stimulated with 100 nmol/L of SDF-1 first then 100 nmol/L of Kp-10 can fully respond to each ligand. *B-E*, the cells were exposed to either HBSS (*B*) or 1 nmol/L Kp-10 (*C*), 10 nmol/L Kp-10 (*D*), or 100 nmol/L Kp-10 (*E*; *first arrow*) followed by 100 nmol/L of SDF-1 (*second arrow*). The response to SDF-1 was almost completely abolished after exposure to 1 nmol/L of Kp-10 and was undetectable with higher concentrations. Representative of at least three independent experiments. Similar results were obtained in HeLa-GPR54 cells.